\mathcal{U}_{z_i}



Autonomous Spacecraft Attitude Reorientation Using Robust Sampled-Data Control Barrier Functions

University of Michigan, Ann Arbor, Michigan 48104

https://doi.org/10.2514/1.G007456

This paper presents a provably safe method for constrained reorientation of a spacecraft in the presence of input constraints, bounded disturbances, and fixed frequency zero-order-hold (ZOH) control inputs. The set of states satisfying all pointing and rate constraints, herein called the safe set, is expressed as the intersection of the sublevel sets of several constraint functions, which are subsequently converted into control barrier functions (CBFs). The method then extends prior results on utilizing CBFs with ZOH controllers to the case of relative-degree-2 constraint functions, as occurs in the constrained attitude reorientation problem. The developed sampled-data controller is also shown to remain provably safe in the presence of input constraints and bounded disturbances. Finally, the method is validated and compared to three prior approaches via both low-fidelity and mid-fidelity simulations.

Nomenclature			
f_1, f_2, g_1, g_2	=	arbitrary functions in model definition	
\mathcal{H}_i	=	inner constraint set corresponding to h_i ,	
		index potentially omitted	
\mathcal{H}_i^{Δ}	=	subset of inner constraint set correspond-	
·		ing to h_i with margin Δ , index potentially	
		omitted	
h_i	=	generic control barrier function, index	
		potentially omitted	
$M_1, M_2, M_2^{\text{alt}}$	=	constants of a constraint function of rela-	
-		tive degree 1	
$M_2^-, M_2^+, M_3^-, M_3^+$	=	constants of a constraint function of rela-	
		tive degree 2	
$p_{\eta}, p_{\eta}^{\mathrm{alt}}$	=	polynomials that upper bound evolution of	
• •		a constraint function of relative degree 1	
p_{κ}, p_h	=	polynomials that upper bound evolution of	
		a constraint function of relative degree 2	
\mathcal{Q}_i	=	constraint set corresponding to κ_i , index	
		potentially omitted	
\mathcal{Q}_i^δ	=	subset of constraint set corresponding to κ_i	
		with margin δ , index potentially omitted	
\boldsymbol{q}	=	state coordinates in Eq. (1), also used as	
		quaternion in Eq. (2)	
8	=	safe set (intersection of constraint sets)	
$ssq: \mathbb{R} \to \mathbb{R}$	=	$ssq(\lambda) = \lambda \lambda $ (ssq is monotone increasing,	
		invertible, and once continuously differ-	
_		entiable)	
T	=	time step of discretization	
\mathbb{T}	=	set of considered times	
t	=	time (arbitrary units)	
t_s	=	specific time instance on a trajectory (see	
		also σ)	
t_0	=	initial time	
\mathcal{U}	=	set of allowable control inputs	

Received 1 January 2023; revision received 17 April 2023; accepted for
publication 18 April 2023; published online 23 June 2023. Copyright © 2023
by the American Institute of Aeronautics and Astronautics, Inc. All rights
reserved. All requests for copying and permission to reprint should be sub-
mitted to CCC at www.copyright.com; employ the eISSN 1533-3884 to
initiate your request. See also AIAA Rights and Permissions www.aiaa.org/
randp.

control input

set of guaranteed safe control inputs for the

ith constraint, index potentially omitted

\mathcal{V}_i	=	constraint set corresponding to η_i , index potentially omitted
v	=	state velocities in Eq. (1)
•		* * *
w	=	vector of wheel states w_i in Eq. (2)
	=	set of possible states
<i>x</i>	=	full state vector x is equal to (q, v)
Z	=	inverse of combined matrix of moments of inertia
$Z_{11}, Z_{12}, Z_{21}, Z_{22}$	=	submatrices of Z
\mathcal{Z}_i	=	robust inner constraint set corresponding
		to κ_i or η_i , index potentially omitted
η_i	=	generic relative-degree-1 constraint func-
11		tion, index potentially omitted
κ_i	=	generic relative-degree-2 constraint func-
•		tion, index potentially omitted
μ	=	parameter used to define control barrier
		functions for relative-degree-2 constraints
Ξ	=	set of considered disturbances
Ξ ξ	=	perturbing input
σ	=	specific time instance on a trajectory (see
		also t_s)
τ	=	arbitrary number in $\mathbb{R}_{>0}$
ϕ	=	function for $\dot{\eta}$ under no disturbances
ϕ_1, ϕ_2	=	functions used for constructing relative-
71772		degree-1 safety conditions
Ψ	=	function for $\ddot{\kappa}$ under no disturbances
ω	=	angular velocity state in Eq. (2)
(,),[,]	=	open interval, closed interval
5 - 2 - E - 2		•

I. Introduction

HIS paper extends the recent theory of control barrier functions (CBFs) to solve the problem of constrained spacecraft attitude reorientation. At present, most spacecraft reorientations are accomplished either via shortest-path maneuvers, which can be easily implemented onboard a spacecraft, or else are preplanned by ground operators when more complex maneuvers are required. As the number of active spacecraft increases, there is potential for reducing operating costs in the latter case by increasing spacecraft autonomy, i.e., by computing maneuvers onboard without consulting ground operators. A common scenario in which shortest-path maneuvers are not allowable is when a spacecraft is not permitted to point sensitive instruments (body-fixed vectors) at bright objects (inertially fixed vectors), or equivalently, when a spacecraft is required to keep an instrument pointed in a specified direction.

The problem of constrained reorientation has been studied extensively, using methods including path planners [1–10], model predictive controllers (MPCs) [11-15], sliding mode controllers (SMCs) [16–18], reference governors [19], and barrier functions [20–24]. It has also been studied using CBFs combined with path planning

^{*}Ph.D. Candidate, Department of Aerospace Engineering; jbreeden@ umich.edu. Student Member AIAA (Corresponding Author).

Associate Professor, Department of Robotics and Department of Aerospace Engineering; dpanagou@umich.edu. Member AIAA.

in [25], along with cursory treatment using CBFs with controllers computed online in [26–29]. Compared to prior approaches, this paper develops a method that provably guarantees both state constraint (i.e., instrument pointing requirements are obeyed) and input constraint (i.e., maximum allowable torques are not exceeded) satisfaction in the presence of bounded disturbances and under a sampled-data control law. The final control law is the output of a four-dimensional quadratic program (QP) that is computationally lightweight. These guarantees are particularly useful when designing SmallSat attitude controllers, which often operate with infrequent ground contact, using undersized actuators (i.e., tight input constraints), at low altitudes (i.e., large disturbances), at low control sampling frequencies, and with limited computational capabilities.

To employ standard CBF terminology, we refer to the set of states with allowable separations between all instruments and all bright objects, and with allowable angular rates, as the safe set, which we assume to be nonempty at all times. The central problem is that of rendering trajectories always inside the safe set from some viable set [30] of initial conditions where this problem is well-posed.

Early work on constrained reorientation in [20] developed a Lyapunov function for safe reorientation in terms of Euler angles, though this Lyapunov function may be nonconvex. The authors in [1] noted that this same constraint could be expressed as a convex set of quaternions, and in [21,22] authors developed a strictly convex Lyapunov function in terms of quaternions. The work in [17,18] added an angular velocity constraint and actuator-allocation algorithm to the same technique. The work in [24] expanded the technique to modified Rodrigues parameters and proposed a method for ensuring input constraint satisfaction. Note that, while these Lyapunov functions resulted in simple control laws that could be implemented online, none of these approaches consider controller sampling, and these controllers can result in slow trajectories, as we show in Sec. V.

An early path-planning technique utilized a variant of rapidly exploring random trees to find safe paths in SO(3) space [10]. Later, path-planning techniques using direct optimization along with the quaternion constraint identified in [1] were developed in [1,2,6] and combined with translational planning in [5], though these methods are potentially too computationally intensive to implement online on a spacecraft processor. Related work in [3,4,8] discretized the safe set to a finite set of nodes and used graph search techniques to plan paths between the nodes. The maneuvers resulting from these techniques are safe but possibly inefficient due to the discretization. The planners in [7,9] add additional refinements to improve efficiency, whereas the controller proposed in [25] executes a faster transition between the path nodes and uses CBFs to keep the trajectory within a safe region around the preplanned path. By comparison, the approach employed in this work and in [21,22] only keeps the state away from unsafe states rather than in a neighborhood of a precomputed safe path as in [25].

MPC approaches to constrained reorientation, such as [11] and its extensions in [12,13], are generally special applications of pathplanning techniques. Similarly, the SMC approach in [16-18] and the approximate optimal control via reinforcement learning in [23] are special applications of the barrier functions used in [21,22]. While MPC and optimal control can provide safety guarantees, in this paper, we seek a method that is less computationally intensive. The reference governor approach in [19] is notable because it developed an explicit control law without path planning that is guaranteed to satisfy input constraints. However, few of the aforementioned approaches explicitly consider disturbances, whereas there is extensive CBF literature on disturbance rejection [31,32], and a recent result on simultaneous disturbance rejection and input constraint satisfaction [33]. Finally, spacecraft often operate with digital controllers with slow update cycles. Path planners and MPC can account for controller sampling given sufficiently sophisticated models, while most Lyapunov methods cannot. On the other hand, margins for controller sampling have also been considered in prior CBF literature such as [29,34], which this paper will extend to also account for relative-degree-2 state constraints, input constraints, and disturbance rejection.

CBFs are a Lyapunov-like method for determining safe control inputs, i.e., control inputs that generate trajectories that provably satisfy the state constraints. For an overview of CBFs, see [35]. In

this methodology, we assume that each requirement that the system trajectories must satisfy is expressed as the state belonging to a given constraint set (e.g., the set of states such that a particular instrument is sufficiently far away from a particular bright object). The safe set is then the intersection of all constraint sets [36,37]. For each constraint set, we then construct a corresponding CBF (e.g., [33,38,39]) and associated zero-sublevel set, herein called an inner constraint set. Each CBF then provides a pointwise condition on the control input that is sufficient to ensure that state trajectories always belong to the CBF's inner constraint set. Multiple CBFs and inner constraint sets may then be combined to establish forward invariance of a subset of the safe set [36,37]. Application of CBFs to attitude control was first suggested in [27], and in fact, it would be simple to express the quaternion constraint developed in [1] as a CBF. However, such a CBF would suffer from the same challenges with input constraints, disturbances, and controller sampling as the related Lyapunov approaches in [17,18,21,22]. These challenges are amplified when some of the constraint functions are of relative degree 2 with respect to the system dynamics, as is the case for spacecraft pointing constraints. That said, extensions of [35] in the CBF literature provide several general tools for addressing these challenges [29,31–33, 35,40,41], as well as other potentially relevant phenomena not presently considered. The authors have recently addressed input constraint satisfaction, robustness to disturbances, and zero-order-hold (ZOH) controller sampling with CBFs individually in [29,33,41], and will incorporate and extend all of these results in this paper. In particular, we will show in Example 1 that the ZOH discretization method in [29] is not immediately compatible with the input constraint work in [33,40,41], so the bulk of Sec. III is devoted to reconciling these two approaches while minimizing conservatism. We then apply all the CBF conditions together online using an m-dimensional (QP), where m is the number of control inputs and is generally far smaller than the dimension of the optimizations in planning or MPC approaches.

The rest of this paper is organized into both 1) a general method accomplishing the above foci for arbitrary systems and constraints, and 2) a case study that applies this method to the constrained reorientation problem. The case study is presented in parallel as each step of the theory is developed for numerical motivation. Section II presents the formulation of the general problem, and of the specific system and constraints used in the case study. Section III presents the main result combining ZOH control inputs [29] with input constraints [33,40,41] and disturbances [31,33] for relative-degree-2 constraints (e.g., pointing constraints), while Sec. IV presents a related extension of [29] for relative-degree-1 constraints (e.g., angular rate constraints). Section V presents the real-time QP controller and simulations both in MATLAB and in a NASA-developed attitude control simulator. Section VI presents concluding remarks. Proofs of the theorems in Secs. III and IV are contained in the Appendix.

II. Preliminaries and Problem Formulation

A. Model

Drawing upon [37], let $q \in \mathbb{Q} \subseteq \mathbb{R}^{n_1}$ be the coordinates and $v \in \mathbb{V} \subseteq \mathbb{R}^{n_2}$ the velocities of a second-order system:

$$\dot{\mathbf{q}} = f_1(t, \mathbf{q}, \mathbf{v}) \tag{1a}$$

$$\dot{\boldsymbol{v}} = f_2(t, \boldsymbol{q}, \boldsymbol{v}) + g_1(t, \boldsymbol{q}, \boldsymbol{v})\boldsymbol{u} + g_2(t, \boldsymbol{q}, \boldsymbol{v})\boldsymbol{\xi}$$
 (1b)

with time $t \in \mathbb{T} \subseteq \mathbb{R}$, state $\mathbf{x} \triangleq (\mathbf{q}, \mathbf{v}) \in \mathbb{X} \triangleq \mathbb{Q} \times \mathbb{V} \subseteq \mathbb{R}^{n_1 + n_2}$, and control $\mathbf{u} \in \mathcal{U} \subset \mathbb{R}^m$, where \mathcal{U} is compact, and disturbance $\mathbf{\xi} \in \Xi \subset \mathbb{R}^p$, where Ξ is bounded. Assume that function f_1 is twice continuously differentiable in all arguments, that functions f_2, g_1, g_2 are continuously differentiable in all arguments, and that $f_1, f_2, g_1, g_2, \mathbf{u}, \mathbf{\xi}$ are sufficiently regular so as to admit unique system trajectories for the entire time domain \mathbb{T} . The results of this paper hold for general f_1, f_2, g_1, g_2 , but we are most interested in applications to attitude control, so suppose the following specific system.

Case Study Part i (System Definition): Assume a single rigid-body spacecraft. Let F_N be an inertial frame and F_B a spacecraft-fixed

Table 1 Physical parameters of the spacecraft

Parameter	Value			
m	4			
A	$ \begin{bmatrix} 0 & 0 & 0.8165 & -0.8165 \\ 0 & -0.9428 & 0.4714 & 0.4714 \\ -1 & 0.3333 & 0.3333 & 0.3333 \end{bmatrix} $			
$\boldsymbol{J}_{w,i}$	$1.722(10)^{-5} \text{ kg} \cdot \text{m}^2, i = 1, 2, 3, 4$			
$u_{\max,i}$	$7(10)^{-4} \text{ N} \cdot \text{m}, i = 1, 2, 3, 4$			
J_b	$\begin{bmatrix} 0.1672 & 0 & 0 \\ 0 & 0.1259 & 0 \\ 0 & 0 & 0.06121 \end{bmatrix} \text{kg} \cdot \text{m}^2$ $\begin{bmatrix} 0.1672 & P_{12} & P_{13} \\ P_{21} & 0.1259 & P_{23} \\ P_{31} & P_{32} & 0.06121 \end{bmatrix} \text{kg} \cdot \text{m}^2$ where $ P_{ij} < 10^{-20}$ for $i \neq j$			
$e_{ m max} \ w_{ m max} \ \xi_{ m max}$	5.092(10) ⁻⁵ kg·m ² /s ² 628.3 rad/s 1.00(10) ⁻⁵ N·m			

frame. For this case study, let $\mathbb{Q} = \{q \in \mathbb{R}^4 | ||q|| = 1\}$ be the quaternion space and let $\mathbf{q} = [q_0, q_1, q_2, q_3]^T \in \mathbb{Q}$ be the quaternion (with scalar element q_0 first) that rotates from F_N to F_B . Let $\omega \in$ \mathbb{R}^3 be the angular velocity of F_B with respect to F_N expressed in frame F_B . Suppose that the spacecraft has m reaction wheels. Let $\boldsymbol{a}_i, i = 1, \dots, m, \ \boldsymbol{a}_i \in \mathbb{R}^3, \ \|\boldsymbol{a}_i\| = 1,$ denote the spin axes of the wheels in frame F_B , and define $A \in \mathbb{R}^{3 \times m}$ as $A \triangleq [a_1, \dots, a_m]$. Let $w_i, i = 1, \dots, m, w_i \in \mathbb{R}$, denote the angular velocity of the wheels with respect to F_B , and define $\mathbf{w} \in \mathbb{R}^m$ as $\mathbf{w} = [w_1, \dots, w_m]^T$. The system velocities as in Eq. (1b) are $\mathbf{v} = (\boldsymbol{\omega}, \mathbf{w}) \in \mathbb{V} = \mathbb{R}^{3+m}$. Assume that each wheel is axially symmetric and let $J_{w,i} \in \mathbb{R}_{>0}$ be the axial moment of inertia of the *i*th wheel, and let $J_w \in \mathbb{R}^{m \times m}$ be a diagonal matrix whose *i*th row and column element is $J_{w,i}$. Let J_b be the moment of inertia of the spacecraft without wheels plus the transverse moments of inertia of the wheels (e.g., see [42] (Eq. 3.140, Chap. 3.3.5.1)) expressed in frame F_B , and let $J_{\text{tot}} \triangleq$ $J_b + \sum_{i=1}^m J_{w,i}(\boldsymbol{a}_i \boldsymbol{a}_i^T)$ denote the total moment of inertia of the spacecraft. Assume that J_b and J_w are constant. The spacecraft state is then $\mathbf{x} = (\mathbf{q}, \boldsymbol{\omega}, \mathbf{w}) \in \mathbb{X} = \mathbb{Q} \times \mathbb{R}^{3+m}$ and the dynamics [43] are

$$\dot{q} = \frac{1}{2} \begin{bmatrix} 0 & -\omega_1 & -\omega_2 & -\omega_3 \\ \omega_1 & 0 & \omega_3 & -\omega_2 \\ \omega_2 & -\omega_3 & 0 & \omega_1 \\ \omega_3 & \omega_2 & -\omega_1 & 0 \end{bmatrix} q$$
 (2a)

$$\begin{bmatrix} \dot{\boldsymbol{\omega}} \\ \dot{\boldsymbol{w}} \end{bmatrix} = \underbrace{\begin{bmatrix} J_{\text{tot}} & AJ_w \\ J_wA^T & J_w \end{bmatrix}^{-1}}_{\triangleq Z} \begin{bmatrix} -\boldsymbol{\omega} \times (J_{\text{tot}}\boldsymbol{\omega} + AJ_w\boldsymbol{w}) + \boldsymbol{\xi} \\ \boldsymbol{u} \end{bmatrix}$$
(2b)

where $\boldsymbol{u} \in \mathcal{U} \subset \mathbb{R}^m$ is the commanded wheel torque. The maximum wheel torque is limited to u_{\max} , so $\mathcal{U} = \{\boldsymbol{u} \in \mathbb{R}^m | \|\boldsymbol{u}\|_{\infty} \leq u_{\max}\}$. For this particular case study, we suppose a 6U CubeSat with parameters given in Table 1 and visualized in Fig. 1. Note that we have chosen a configuration with four wheels in Table 1 rather than a more typical three-wheel configuration in order to demonstrate the general applicability of these results. The wheel moments of inertia and maximum torques in Table 1 are based off a commercially available wheel package, with the maximum per-wheel torque reduced to be comparable to a three-wheel configuration. Let $\Xi = \{\boldsymbol{\xi} \in \mathbb{R}^3 | \|\boldsymbol{\xi}\| \leq \xi_{\max}\}$ for ξ_{\max} in Table 1, which comes from approximate values of aerodynamic drag on a 6U CubeSat at 500 km altitude.

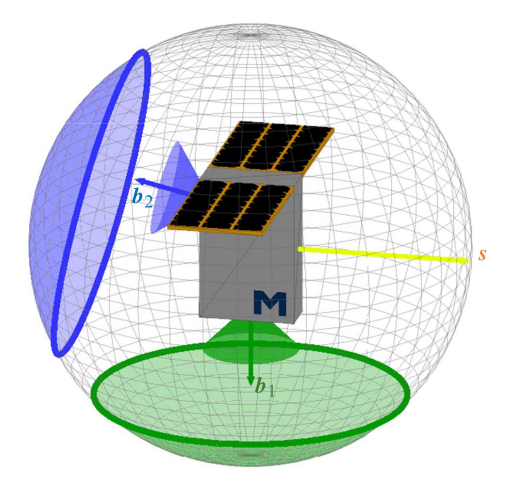


Fig. 1 A 6U CubeSat with two spacecraft-fixed keep-out zones centered about b_1 , b_2 , and an inertially fixed vector s that must be kept outside these zones.

B. Safety Constraints

Next, suppose that the trajectories of Eq. (1) are required to lie in the intersection of several constraint sets, each defined by the zero sublevel set of some constraint function. Let $\kappa_i \colon \mathbb{T} \times \mathbb{Q} \to \mathbb{R}$ for $i = 1, \ldots, N_1$ denote the relative-degree-2 constraint functions, and let $\eta_i \colon \mathbb{T} \times \mathbb{V} \to \mathbb{R}$ for $i = N_1 + 1, \ldots, N_1 + N_2$ denote the relative-degree-1 constraint functions. The constraint sets are

$$Q_i(t) \triangleq \{x = (q, v) \in \mathbb{X} | \kappa_i(t, q) \le 0\}$$
 (3a)

$$\mathcal{V}_i(t) \triangleq \{ \mathbf{x} = (\mathbf{q}, \mathbf{v}) \in \mathbb{X} | \eta_i(t, \mathbf{v}) \le 0 \}$$
 (3b)

and the resultant safe set is

$$S(t) \triangleq \left(\bigcap_{i=1}^{N_1} Q_i(t)\right) \cap \left(\bigcap_{i=N_1+1}^{N_1+N_2} V_i(t)\right) \tag{4}$$

where Q_i , V_i , and S are permitted to be time-varying. As an abuse of notation, we will generally write $\kappa_i(t, \mathbf{x})$ and $\eta_i(t, \mathbf{x})$ in place of $\kappa_i(t, \mathbf{q})$ and $\eta_i(t, \mathbf{v})$ in order to match the CBF notation in Sec. II.C. Some constraint functions that are common in attitude control are as follows; these constraints are also the basis of our simulations in Sec. V.

Case Study Part ii (Constraints): For the spacecraft system in Eq. (2), let $b \in \mathbb{R}^3$, ||b|| = 1, be a body-fixed vector, such as an instrument boresight vector (e.g., the green or blue vectors in Fig. 1). Let s(t), ||s(t)|| = 1, be a vector, potentially time-varying (provided s is thrice continuously differentiable), for which we require that the angle between s(t) and b is always at least θ (e.g., the local sun vector, represented by the yellow vector in Fig. 1). This leads to a constraint function of the form

$$\kappa_b(t, \mathbf{q}) = \mathbf{s}(t)^T R(\mathbf{q}) \mathbf{b} - \cos \theta \tag{5}$$

where R(q) is

$$R(\mathbf{q}) \triangleq \begin{bmatrix} 1 - 2q_2^2 - 2q_3^2 & 2q_1q_2 - 2q_0q_3 & 2q_0q_2 + 2q_1q_3 \\ 2q_0q_3 + 2q_1q_2 & 1 - 2q_1^2 - 2q_3^2 & 2q_2q_3 - 2q_0q_1 \\ 2q_1q_3 - 2q_0q_2 & 2q_0q_1 + 2q_2q_3 & 1 - 2q_1^2 - 2q_2^2 \end{bmatrix}$$

$$(6)$$

This is a relative-degree-2 constraint function, since $\dot{\kappa}_b$ is not a function of u, ξ . Note that Eq. (5) can be used to express both keep-out and keep-in zones. Also note that κ_b in Eq. (5) is equivalent to $\kappa_b^*(t, q) = q^{*T}Mq^*$ in [1] (Eq. 2.5), where M is given in [1] (Eq. 2.6) and $q^* = [-q_1, -q_2, -q_3, q_0]^T$ is the conjugate of q

[‡]CubeWheel Medium: www.cubespace.co.za/products/adcs-components/cubewheel/#cubewheel-specifications.

with the scalar element q_0 last (the conjugate arises because of notational differences with [1]). Next, we also require that the maximum angular rate of the spacecraft is bounded for safety of the spacecraft structure. This leads to the constraint function

$$\eta_{\omega}(t, \mathbf{v}) = \boldsymbol{\omega}^T P \boldsymbol{\omega} - e_{\text{max}} \tag{7}$$

where $e_{\max} \in \mathbb{R}$ and $P \in \mathbb{R}^{3 \times 3}$ are given in Table 1. The values of e_{\max} and P are constructed so that the safe set allows for angular rates of up to 1 deg/s on the largest principal axis and up to 2.730 deg/s on the smallest principal axis, and will be elaborated upon in Case Study Parts xi–xii. This is a relative-degree-1 constraint, since $\dot{\eta}_{\omega}$ is a function of u, ξ . Finally, we require that the wheel angular velocities are limited, so introduce m constraint functions:

$$\eta_{w_i}(t, \mathbf{v}) = |w_i| - w_{\text{max}}, \quad i = 1, \dots, m$$
(8)

where w_{\max} is a constant. This paper will assume that a suitable momentum dumping control law (e.g., scheduled thruster or magnetorquer application) has been developed so that the constraints encoded by $\eta_{w_i}(t,x)$ are always satisfied without impacting the rest of the control design. Thus, we only focus on the relative-degree-1 constraint in η_{ω} and the relative-degree-2 constraint in κ_b , though we still incorporate the wheel rate bounds in Eq. (8) in the safe set construction in Eq. (4). Finally, for this case study, suppose that there are two constraints of the form Eq. (5) for body-fixed vectors \boldsymbol{b}_1 and \boldsymbol{b}_2 , so the safe set is $\mathcal{S} = \mathcal{Q}_{b_1} \cap \mathcal{Q}_{b_2} \cap \mathcal{V}_{\omega} \cap \mathcal{V}_{w_1} \cap \mathcal{V}_{w_2} \cap \mathcal{V}_{w_3} \cap \mathcal{V}_{w_4}$.

C. Continuous-Time CBFs

This paper will utilize and extend CBF theory to address the problem of rendering state trajectories always inside the safe set. A formal definition of CBF with robustness to bounded disturbances is as follows.

Definition 1 ([33] Def. 3): For the system (1), a continuously differentiable function $h_i: \mathbb{T} \times \mathbb{X} \to \mathbb{R}$ is a CBF on the set \mathcal{S} if there exists a locally Lipschitz continuous class- \mathcal{K} function $\alpha_i: \mathbb{R}_{\geq 0} \to \mathbb{R}_{\geq 0}$ such that

 $\sup_{\boldsymbol{\xi} \in \Xi} \min_{\boldsymbol{u} \in \mathcal{U}} \dot{h}_i(t, \boldsymbol{x}, \boldsymbol{u}, \boldsymbol{\xi}) \leq \alpha_i(-h_i(t, \boldsymbol{x})), \quad \forall \boldsymbol{x} \in \mathcal{H}_i(t) \cap \mathcal{S}(t), \ \forall t \in \mathbb{T}$

(9)

where \mathcal{H}_i is called the inner constraint set and is given by

$$\mathcal{H}_i(t) \triangleq \{ x \in \mathbb{X} | h_i(t, x) \le 0 \}$$
 (10)

That is, a scalar-valued function h_i is a CBF if there is sufficient control authority given the set \mathcal{U} that the total derivative of h_i can be upper bounded regardless of the disturbance value $\boldsymbol{\xi}$ in the considered set Ξ . The following lemma, derived from [33] (Lemma 4) and [37] (Lemma 3), can then be used to guarantee forward invariance (i.e., safety) of the set \mathcal{H}_i .

Lemma 1: Let u(t, x) be a control law. Given a CBF h_i on S satisfying Definition 1, if $x(t_0) \in \mathcal{H}_i(t_0)$ and u satisfies

$$\sup_{\boldsymbol{\xi} \in \Xi} \dot{h}_i(t, \boldsymbol{x}(t), \boldsymbol{u}(t, \boldsymbol{x}(t)), \boldsymbol{\xi}) \le \alpha_i(-h_i(t, \boldsymbol{x}(t))) \tag{11}$$

for all $t \in [t_0, t_f)$, where t_f is possibly ∞ , then x(t) remains in $\mathcal{H}_i(t)$ for all $t \in [t_0, t_f)$.

That is, as long as the control law satisfies the condition (11), called the CBF condition, the state trajectory cannot leave \mathcal{H}_i ; i.e., \mathcal{H}_i is a controlled-invariant set. In general, \mathcal{H}_i is not equivalent to \mathcal{S} , because there may exist states in $\mathcal{S}(t_0)$ that are instantaneously safe at t_0 , but that cannot be rendered safe for all $t \in [t_0, t_f)$ [33]. Thus, we call \mathcal{H}_i an inner constraint set. We note that Lemma 1 can be applied to any number of CBFs, so we seek a collection of CBFs $\{h_i\}_{i=1}^M$ such that $\bigcap_{i=1}^M \mathcal{H}_i$ is a subset of \mathcal{S} in Eq. (4) (see [37] Lemmas 2 and 3). Specifically, our final control law will employ one CBF h_i for each

constraint function κ_i or η_i (equivalently, one CBF set \mathcal{H}_i for each constraint set \mathcal{Q}_i or \mathcal{V}_i) in order to leverage existing literature [33,40,41], though such a one-to-one correspondence is not necessary [37].

Denote the set of control inputs satisfying Eq. (11) as $\mathcal{U}_{h_i}(t, x)$. Note that the total derivative of h_i is

$$\dot{h}_{i}(t, \mathbf{x}, \mathbf{u}, \boldsymbol{\xi}) = \frac{\partial h_{i}(t, \mathbf{x})}{\partial t} + \frac{\partial h_{i}(t, \mathbf{x})}{\partial q} f_{1}(t, \mathbf{x}) + \frac{\partial h_{i}(t, \mathbf{x})}{\partial v} f_{2}(t, \mathbf{x}) + g_{1}(t, \mathbf{x})\mathbf{u} + g_{2}(t, \mathbf{x})\boldsymbol{\xi}$$
(12)

so each condition (11), $i = 1, ..., N_1 + N_2$, is affine in \boldsymbol{u} and each \mathcal{U}_{h_i} is a half-space. Thus, a QP-based control law as in [35] (Sec. II.C) can efficiently solve for \boldsymbol{u} satisfying several constraints of the form Eq. (11) simultaneously.

For each relative-degree-1 constraint η_i in Eq. (3b), we will choose the CBF $h_i \equiv \eta_i$ so $\mathcal{H}_i \equiv \mathcal{V}_i$. For the relative-degree-2 constraints κ_i in Eq. (3a), various methods to construct a CBF h_i such that $\mathcal{H}_i \subseteq \mathcal{Q}_i$ are covered in [33,40,41], and this paper will extend the method in [33] (Sec. 3.1) specifically. For a constraint function κ_i satisfying certain properties (covered in [33] Sec. 3.1), one possible choice of CBF is

$$h_i(t, \mathbf{x}) = \kappa_i(t, \mathbf{x}) + \frac{\dot{\kappa}_i(t, \mathbf{x})|\dot{\kappa}_i(t, \mathbf{x})|}{2\mu}$$
(13)

for some parameter $\mu > 0$. This choice of CBF does not work for all systems, but is particularly useful for systems similar to the double integrator, such as a double integrator with small nonlinearities. We hypothesize that Eq. (13) can be used for pointing constraints as in Eq. (5), so this is the only CBF for relative-degree-2 constraint functions κ_i considered in this paper. Possible extensions of the other CBFs in [33,40] to ZOH control inputs are left to future work.

Let $\mu_1 > \mu_2 > 0$, and let h_{i,μ_1} and h_{i,μ_2} be two corresponding CBFs. Note that $\mathcal{H}_{i,\mu_1} \supset \mathcal{H}_{i,\mu_2}$. Thus, the least conservative CBF of the form (13) will have the largest allowable parameter μ . Also note that with h_i as in Eq. (13), the set \mathcal{H}_i is does not meet our requirement that \mathcal{H}_i is a subset of \mathcal{Q}_i . To address this, we recall the following lemma.

Lemma 2 ([33] Lemma 7): Let u(t, x) be a control law. For some function κ_i , let h_i be as in Eq. (13). If $x(t_0) \in \mathcal{H}_i(t_0) \cap \mathcal{Q}_i(t_0)$ and u satisfies Eq. (11) for all $t \in [t_0, t_f)$, where t_f is possibly ∞ , then x(t) remains in $\mathcal{H}_i(t) \cap \mathcal{Q}_i(t)$ for all $t \in [t_0, t_f)$.

That is, even though Lemma 1 only guarantees forward invariance of \mathcal{H}_i , because of the special form of h in Eq. (13), the set $\mathcal{H}_i \cap \mathcal{Q}_i$ is also rendered forward invariant. We now consider how Eq. (13) applies to our case study.

Case Study Part iii (Continuous-Time CBF): For the constraint function κ_b in Eq. (5), the function h_b in Eq. (13) is a CBF on S as in Definition 1 for any parameter $0 < \mu \le 0.0025$.

D. Robust Sampled-Data Formulation

Thus far, all results have been for continuous controller updates, but our goal is to apply the CBFs (13) and (7) when the controller is instead updated at a fixed frequency. Now suppose that the control input \boldsymbol{u} is updated at discrete times t_k , $k \in \mathbb{N}$, where $t_{k+1} - t_k = T$ for fixed time-step T > 0, and that \boldsymbol{u} is fixed between time steps k and k+1. That is, we seek a ZOH control law

$$\mathbf{u}(t) = \mathbf{u}_k, \quad \forall t \in [t_k, t_{k+1}) \tag{14}$$

where $u_k = u(t_k, x(t_k)) \in \mathcal{U}$. Denote $x_k = x(t_k)$. Since the control input is updated only at the times t_k , it is difficult to ensure that Eq. (11) is satisfied at every time instant (i.e., including between time steps), as is required for Lemma 1 to apply. The work in [29] summarizes three stricter versions of Eq. (11) that when applied only at times $t_k, k \in \mathbb{N}$ ensures that the original condition (11) is always satisfied between time steps, and a related method that accomplishes the same result without using Eq. (11). However, the methods in [29] do not easily apply to CBFs constructed from relative-degree-2

constraint functions, such as in Eq. (13). This is demonstrated by way of the following example.

Example 1: Given a relative-degree-2 constraint function κ_i , one possible CBF is that in Eq. (13) for some constant $\mu > 0$. According to [29] (Thm. 3), this CBF can be rendered safe in a ZOH fashion if for all $x \in \mathcal{H}_i(t)$, $t \in \mathbb{T}$ there exists $u \in \mathcal{U}$ such that

$$\dot{h}_i(t, \mathbf{x}) = \dot{\kappa}_i(t, \mathbf{x}) \left(1 + \frac{\ddot{\kappa}_i(t, \mathbf{x}, \mathbf{u}, \boldsymbol{\xi})}{\mu} \right) \le -\frac{1}{T} \kappa_i(t, \mathbf{x}) - \frac{1}{2} r T \quad (15)$$

where $r \ge 0$ is a parameter defined in [29] (Eq. (17)). As explained in [29], r could either be a constant ("global" case), or a function of t, x ("local" case) depending on the implementation. In either case, r represents possible values of $\ddot{\kappa}_i$ and, for that reason, is usually lower bounded by a positive number, here denoted $r_0 > 0$ (in the global case, let $r_0 = r$).

The issue that arises here is that, for any arbitrarily small $\delta > 0$, there exist $\mathbf{x} \in \mathcal{H}_i(t), t \in \mathbb{T}$ such that $\dot{\kappa}_i(t, \mathbf{x}) = \delta$ and $\kappa_i(t, \mathbf{x}) = -\frac{\delta^2}{2\mu}$. For such \mathbf{x} , Eq. (15) simplifies to

$$\ddot{\kappa}_i(t, \boldsymbol{x}, \boldsymbol{u}, \boldsymbol{\xi}) \le \epsilon(\delta) \triangleq \frac{\delta}{2T} - \frac{\mu r T}{2\delta}$$

Because $r \geq r_0 > 0$, it follows that $\lim_{\delta \to 0^+} \epsilon(\delta) = -\infty$. That is, the ZOH sampling margin r causes the required $\ddot{\kappa}_i$ to go to $-\infty$ near the boundary of \mathcal{H}_i , which also causes the required \boldsymbol{u} to become unbounded. Thus, the methods in [29] cannot be applied to the CBF (13), or any of the relative-degree-2 strategies in [33], if there are also input constraints.

Thus, the method in [29] suffers from the infeasibility of the condition [29] (Eq. 5) when the control input u is constrained. The interested reader can examine this problem further by downloading the code linked in [29] and increasing the value of the constant μ in [29] (Table 1). Thus, the central problem of this paper is as follows.

Problem 1: Given the safe set \mathcal{S} in Eq. (4), focus on a single constraint function $\eta_i : \mathbb{T} \times \mathbb{V} \to \mathbb{R}$ or $\kappa_i : \mathbb{T} \times \mathbb{Q} \to \mathbb{R}$ that is of relative degree 1 or 2, respectively, with respect to the dynamic model (1). Assume that $\mathbf{x}(t_k) \in \mathcal{S}(t_k)$ in Eq. (4) at the current sample time k, and that all other constraints $\mathbf{x}(t) \in \mathcal{Q}_j(t)$ and $\mathbf{x}(t) \in \mathcal{V}_j(t)$ for $j \neq i$ are satisfied for all t in the inter-sample period $[t_k, t_{k+1})$. We seek to derive a set $\mathcal{Z}_i(t) \subseteq \mathcal{Q}_i(t)$ or $\mathcal{Z}_i(t) \subseteq \mathcal{V}_i(t)$ for all $t \in \mathbb{T}$ and a set $\mathcal{U}_{z_i}(t_k, \mathbf{x}(t_k))$ such that 1) given $\mathbf{x}(t_k) \in \mathcal{Z}_i(t_k)$ and $\mathbf{u}(t_k, \mathbf{x}(t_k)) \in \mathcal{U}_{z_i}(t_k, \mathbf{x}(t_k))$ we can provably guarantee i) $\mathbf{x}(t_{k+1}) \in \mathcal{Z}_i(t_{k+1})$ and ii) $\mathbf{x}(t) \in \mathcal{Q}_i(t)$ or $\mathbf{x}(t) \in \mathcal{V}_i(t)$ for all $t \in [t_k, t_{k+1})$ for any allowable disturbance $\mathbf{\xi} \in \Xi$, and 2) the set $\mathcal{U} \cap \mathcal{U}_{z_i}(t_k, \mathbf{x}(t_k))$ is nonempty for all $\mathbf{x}(t_k) \in \mathcal{Z}_i(t_k) \cap \mathcal{S}(t_k)$, $t_k \in \mathbb{T}$.

We refer to set \mathcal{Z}_i as the *i*th robust inner constraint set. Similar to how we restricted the constraint set \mathcal{Q}_i to the inner constraint set \mathcal{H}_i to account for input constraints, leading to the safe control set \mathcal{U}_{h_i} , in this paper, we will further restrict the allowable sampled states to the new set \mathcal{Z}_i to account for disturbances and controller sampling, leading to the new safe control set \mathcal{U}_{z_i} . Figure 2 shows the relation between \mathcal{Q}_i (cyan), \mathcal{H}_i (hashed), and \mathcal{Z}_i (gray) for a relative-degree-2 constraint function. Section III will address the relative-degree-2 case of Problem 1, while Sec. IV will address the simpler relative-degree-1 case.

III. Method for Relative Degree Two

A. Strategy

We begin by addressing the relative-degree-2 case of Problem 1, as the relative-degree-1 case easily follows. In this section, we drop the subscript i, so let κ denote any relative-degree-2 constraint function [e.g., Eq. (5)], and h the corresponding CBF as in Eq. (13). The core idea of this method, and those in [29,34], is that given $h(t_k, \mathbf{x}(t_k)) \leq 0$, we want to identify a formula for a worst-case value of $h(t_k + \tau, \mathbf{x}(t_k + \tau))$, denoted $h_{\text{bound}}(t_k, \mathbf{x}(t_k), \tau)$, for $\tau \in [0, T]$ and find a suitable control input to ensure that $h_{\text{bound}}(t_k, \mathbf{x}(t_k), \tau)$ is nonpositive for all $\tau \in [0, T]$. However, the problem highlighted in Example 1 is that the worst-case formulas h_{bound} following from

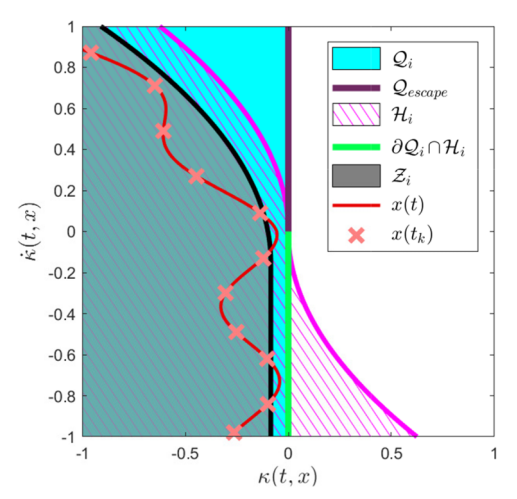


Fig. 2 Diagram of a constraint set \mathcal{Q}_i , corresponding inner constraint set \mathcal{H}_i , robust inner constraint set \mathcal{Z}_i , and a safe trajectory $x(t) \in \mathcal{Q}_i \cap \mathcal{H}_i$ with controller samples $x(t_k) \in \mathcal{Z}_i$ at the red "x" marks.

all the methods in [29,34] rely upon linear approximations of h on the interval $[t_k,t_{k+1}]$. The obvious extension is to use a higher-order approximation of the worst-case trajectory that h could follow between time steps. However, when using a higher-order approximation, it is no longer sufficient to only check that $h_{\text{bound}}(t_k, \boldsymbol{x}(t_k), T) \leq 0$, as there may exist $\tau \in (0, T)$ such that $h_{\text{bound}}(t_k, \boldsymbol{x}(t_k), \tau) > h_{\text{bound}}(t_k, \boldsymbol{x}(t_k), T)$, as visualized by the red and cyan points in Fig. 3. Thus, unlike in [29,34], we must instead check that $h_{\text{bound}}(t_k, \boldsymbol{x}(t_k), \tau) \leq 0$ for all $\tau \in [0, T]$, which adds complexity to the problem. To address this possibility of exiting and returning to the inner constraint set, we seek local maximizers σ (e.g., the red circle in Fig. 3) such that $h_{\text{bound}}(t_k, \boldsymbol{x}(t_k), \sigma) \geq h_{\text{bound}}(t_k, \boldsymbol{x}(t_k), \tau)$ for all $\tau \in [0, T]$. We then identify a bound Δ on the differences $h_{\text{bound}}(t_k, \boldsymbol{x}(t_k), \sigma) - h(t_k, \boldsymbol{x}(t_k))$ and $h_{\text{bound}}(t_k, \boldsymbol{x}(t_k), \tau)$ and define the sets

$$\mathcal{H}^{\Delta}(t) \triangleq \{ x \in \mathbb{X} | h(t, x) \le -\Delta \} \tag{16}$$

$$Q^{\delta}(t) \triangleq \{x \in \mathbb{X} | \kappa(t, x) \le -\delta\}$$
 (17)

It follows that if $h(t_k, \mathbf{x}(t_k)) \leq -\Delta$ and $h_{\text{bound}}(t_k, \mathbf{x}(t_k), T) \leq -\Delta$, which are relatively simple conditions to enforce [e.g., see Eq. (29)], then $h(t_k + \tau, \mathbf{x}(t_k + \tau)) \leq h_{\text{bound}}(t_k, \mathbf{x}(t_k), \tau) \leq h_{\text{bound}}(t_k, \mathbf{x}(t_k), \sigma) \leq 0$ for all $\tau \in [0, T]$. This is visualized in Fig. 2, where the red sample trajectory is always safe, because at the sample times t_k , the trajectory meets the stricter condition of being in the gray set.

To define a set \mathcal{Z} as in Problem 1, we will need expressions for suitable Δ in Eq. (16) and δ in Eq. (17), from which it will follow that $\mathcal{Z} = \mathcal{H}^{\Delta} \cap \mathcal{Q}^{\delta}$. We seek to minimize conservatism, i.e., to choose the smallest δ , Δ for which we can still provably demonstrate safety between each t_k and t_{k+1} . To this end, Secs. III.C and III.D study possible expressions for δ , Δ that work well for the system (2), and that lead to a final control strategy summarized in Theorem 4.

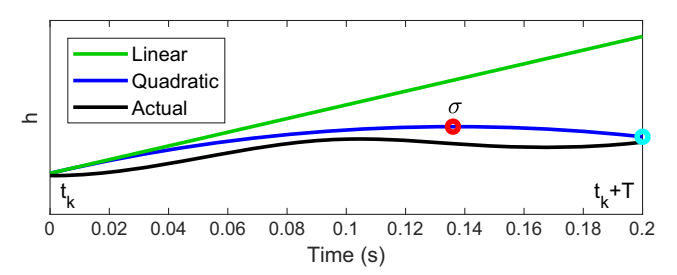


Fig. 3 Diagram of a linear and quadratic upper bound on the trajectory of h(t, x(t)) between two sampled times, and the maximizer σ of the quadratic curve.

Table 2 System constants for case study

Parameter	Value	
T	0.2 s	
M_2^+	$1.64(10)^{-4}$	
M_2^-	$-1.64(10)^{-4}$	
M_3^+	$6.2(10)^{-3}$	
M_3^-	$-6.2(10)^{-3}$	
δ_1	$1.10(10)^{-5}$	
δ_2	$9.7(10)^{-6}$	
Δ_2	$1.3(10)^{-5}$	
Δ_3	$1.09(10)^{-5}$	
μ	0.00167	
M_1	$5.79(10)^{-7}$	
$M_2^{ m alt}$	$1.95(10)^{-5}$	

We begin by presenting a naive approach to determining Δ , δ . Assuming a second-order h_{bound} function [such as that in Eq. (28)], the required margin Δ can be determined entirely by the values of the second derivative \ddot{h} . Thus, consider the following (very conservative) baseline example with numbers derived from our case study.

Case Study Part iv (A Naive Approach to Computing Maximum Overshoot): Let the time step for the controller of Eq. (2) be T=0.2 s. Let h_b as in Eq. (13) be a CBF for κ_b in Eq. (5) and suppose that $\mu=0.00167$ as in Table 2 (which we will justify later). Suppose that $\xi \equiv 0$ for this example. Let $r=\min_{\mathbf{x}\in S(t),t\in \mathbb{T},\mathbf{u}\in \mathcal{U}}\ddot{h}_b(t,\mathbf{x},\mathbf{u},\mathbf{0})=-0.550$. It follows that one possible upper bound on the overshoot of h_b between time steps is $\Delta=-\frac{1}{8}T^2r=2.75(10)^{-3}$. We will show in Secs. III.C and III.D that this is over 200 times as conservative as necessary for this system.

B. Sampling and Robustness Constants

We now proceed similarly to [29] by defining several constants of the system, analogous to the Lipschitz constants in [29], and then using these constants to bound system behavior. First, define

$$M_{2}^{-} \triangleq \inf_{t \in \mathbb{T}, x \in \mathcal{S}(t), \xi \in \Xi} \frac{\partial \dot{\kappa}(t, x)}{\partial v} g_{2}(t, x) \xi$$
 (18a)

$$M_{2}^{+} \triangleq \sup_{t \in \mathbb{T}} \sup_{\mathbf{x} \in S(t)} \frac{\partial \dot{\kappa}(t, \mathbf{x})}{\partial \mathbf{v}} g_{2}(t, \mathbf{x}) \boldsymbol{\xi}$$
 (18b)

The constants M_2^+ and M_2^+ represent bounds on our uncertainty in $\ddot{\kappa}$ because of the unknown disturbance. We assume that Eqs. (18) and (21) are well-defined. We represent the component of $\ddot{\kappa}$ that is certain using the function ψ as follows:

$$\psi(t, \mathbf{x}, \mathbf{u}) \triangleq \frac{\partial \dot{\kappa}(t, \mathbf{x})}{\partial t} + \frac{\partial \dot{\kappa}(t, \mathbf{x})}{\partial \mathbf{q}} f_1(t, \mathbf{x}) + \frac{\partial \dot{\kappa}(t, \mathbf{x})}{\partial \mathbf{v}} \left(f_2(t, \mathbf{x}) + g_1(t, \mathbf{x}) \mathbf{u} \right)$$
(19)

so that

$$\ddot{\kappa}(t, \mathbf{x}, \mathbf{u}) \le \psi(t, \mathbf{x}, \mathbf{u}) + M_2^+ \tag{20a}$$

$$\ddot{\kappa}(t, \mathbf{x}, \mathbf{u}) \ge \psi(t, \mathbf{x}, \mathbf{u}) + M_2^- \tag{20b}$$

In practice, the value of ψ is exactly known only at the sampling times t_k , so we also define the constants

$$M_{3}^{-} \triangleq \inf_{t \in \mathbb{T}, \mathbf{x} \in \mathcal{S}(t), \mathbf{u} \in \mathcal{U}, \boldsymbol{\xi} \in \Xi} \left[\frac{\partial \psi(t, \mathbf{x}, \mathbf{u})}{\partial t} + \frac{\partial \psi(t, \mathbf{x}, \mathbf{u})}{\partial \mathbf{q}} f_{1}(t, \mathbf{x}) \right. \\ \left. + \frac{\partial \psi(t, \mathbf{x}, \mathbf{u})}{\partial \mathbf{v}} \left(f_{2}(t, \mathbf{x}) + g_{1}(t, \mathbf{x}) \mathbf{u} + g_{2}(t, \mathbf{x}) \boldsymbol{\xi} \right) \right]$$
(21a)

$$M_{3}^{+} \triangleq \sup_{t \in \mathbb{T}, \mathbf{x} \in S(t), \mathbf{u} \in \mathcal{U}, \boldsymbol{\xi} \in \Xi} \left[\frac{\partial \psi(t, \mathbf{x}, \mathbf{u})}{\partial t} + \frac{\partial \psi(t, \mathbf{x}, \mathbf{u})}{\partial q} f_{1}(t, \mathbf{x}) \right. \\ \left. + \frac{\partial \psi(t, \mathbf{x}, \mathbf{u})}{\partial v} \left(f_{2}(t, \mathbf{x}) + g_{1}(t, \mathbf{x}) \mathbf{u} + g_{2}(t, \mathbf{x}) \boldsymbol{\xi} \right) \right]$$
(21b)

to describe our uncertainty in the evolution of ψ between time steps due to both the ZOH sampling and the disturbance. That is, for $\tau > 0$,

$$\psi(t+\tau, \mathbf{x}(t+\tau), \mathbf{u}) \le \psi(t, \mathbf{x}(t), \mathbf{u}) + M_3^+ \tau \tag{22a}$$

$$\psi(t+\tau, \mathbf{x}(t+\tau), \mathbf{u}) \ge \psi(t, \mathbf{x}(t), \mathbf{u}) + M_3^{-}\tau \tag{22b}$$

Note that the control input u is the same on both sides of the inequalities in Eq. (22), so these inequalities are only useful during a single ZOH time step. Also, unlike in [29], we assume the bounds $M_2^-, M_2^+, M_3^-, M_3^+$ are global (i.e., are computed over all of S) for simplicity, though extensions for local bounds computed online as in [29] could also be developed at greater computational cost. If the global bounds (18) and (21) are undefined, then more involved analysis than is presently considered may be required. Note that we defined the lower bounds M_2^-, M_3^- and upper bounds M_2^+, M_3^+ separately to cover cases such as when the dynamics and/or disturbance environment are known to tend to increase/decrease h [e.g., if the unsafe state is of higher/lower potential energy than other states, such as would occur if gravity gradient were included in Eq. (2)]. In other cases, it may occur that $M_2^- = -M_2^+$ and $M_3^- = -M_3^+$. In the upcoming theorems, we will need the following relations. Let σ be some time in $[t_k, t_{k+1}]$, where \boldsymbol{u} is constant on $[t_k, t_{k+1})$, and let $\tau \in \mathbb{R}_{\geq 0}$ be such that $\sigma + \tau$ (or $\sigma - \tau$) is also within $[t_k, t_{k+1}]$. Then, using only the time argument for brevity, it holds that

$$\ddot{\kappa}(\sigma) \stackrel{(20a)}{\leq} \psi(\sigma) + M_2^{+} \stackrel{(22b)}{\leq} \psi(\sigma + \tau) - M_3^{-}\tau + M_2^{+} \stackrel{(20b)}{\leq} \ddot{\kappa}(\sigma + \tau) - M_2^{-} - M_3^{-}\tau + M_2^{+}$$
(23a)

$$\ddot{\kappa}(\sigma) \stackrel{\text{(20b)}}{\geq} \psi(\sigma) + M_2^- \stackrel{\text{(22a)}}{\geq} \psi(\sigma + \tau) - M_3^+ \tau + M_2^- \stackrel{\text{(20a)}}{\geq} \ddot{\kappa}(\sigma + \tau) - M_2^+ - M_3^+ \tau + M_2^-$$
(23b)

$$\ddot{\kappa}(\sigma) \stackrel{\text{(20b)}}{\geq} \psi(\sigma) + M_2^{-} \stackrel{\text{(22b)}}{\geq} \psi(\sigma - \tau) + M_3^{-} \tau + M_2^{-} \stackrel{\text{(20a)}}{\geq} \ddot{\kappa}(\sigma - \tau) - M_2^{+} + M_3^{-} \tau + M_2^{-}$$
(23c)

$$\ddot{\kappa}(\sigma) \stackrel{(20a)}{\leq} \psi(\sigma) + M_2^{+} \stackrel{(22a)}{\leq} \psi(\sigma - \tau) + M_3^{+} \tau + M_2^{+} \stackrel{(20b)}{\leq} \ddot{\kappa}(\sigma - \tau) - M_2^{-} + M_3^{+} \tau + M_2^{+}$$
 (23d)

Case Study Part v (Constants): For the system (2) and constraint κ_b in Eq. (5), the values of M_2^- , M_2^+ , M_3^- , M_3^+ are given in Table 2. Note that these values hold for all $\theta \le \pi/2$ in Eq. (5), and are larger than the resultant values (i.e., are overly conservative) when $\theta > \pi/2$.

C. Determining Δ , δ When h and κ Share Maximizers

Using the above constants, we now determine suitable values of Δ , δ for Eqs. (16) and (17) in two parts. First, we note that a necessary condition for a maximizer σ of h occurring between time steps t_k and t_{k+1} is $\dot{h}(\sigma, \mathbf{x}(\sigma), \mathbf{u}_k, \boldsymbol{\xi}) = 0$. Because of the form of h in Eq. (13), a sufficient condition for $\dot{h} = 0$ is $\dot{\kappa} = 0$, so maximizers of h will often be co-located with maximizers of κ , as illustrated by the blue lines in Fig. 4. Thus, this subsection determines appropriate margins Δ , δ specifically when the maximizers of κ and h are co-located, while the following subsection determines these margins when this is not the case (green lines in Fig. 4). We begin with the following lemma.

Lemma 3: Suppose that κ is thrice differentiable and of relative degree 2 with respect to Eq. (1), and \boldsymbol{u} is constant on $[t_k, t_{k+1})$. If $\sigma \in (t_k, t_{k+1})$ is the time of a local maximizer of h in Eq. (13) on (t_k, t_{k+1})

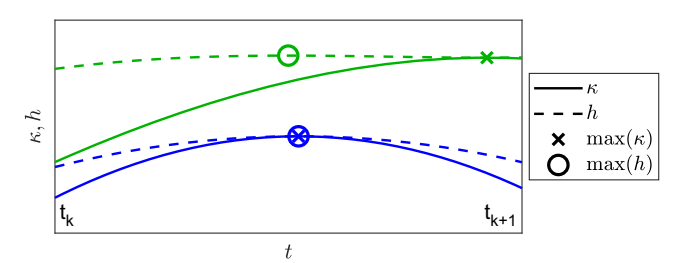


Fig. 4 Illustration of trajectories where the maximizers of κ and h on $[t_k,t_{k+1}]$ are co-located (blue), and where the maximizer of h precedes that of κ (green).

and $\dot{\kappa}(\sigma, \mathbf{x}(\sigma)) = 0$, then σ is also a local maximizer of κ on (t_k, t_{k+1}) and it must hold that $0 \ge \ddot{\kappa}(\sigma, \mathbf{x}(\sigma), \mathbf{u}, \boldsymbol{\xi}) \ge -\mu$.

The consequence of Lemma 3 is that, provided that the stated condition holds, we can now use knowledge about κ to upper bound the variation in h between time steps. Lemma 3 is particularly helpful because analysis of κ is generally simpler than analysis of h, and because μ is a tunable parameter. Note that maximizers of the CBF h can also occur when $\dot{\kappa}(\sigma, \mathbf{x}(\sigma)) \neq 0$ and in these cases Lemma 3 would no longer apply, thus motivating Lemma 4 in Sec. III.D. However, when Lemma 3 does hold, we can substantially reduce the required conservatism to prevent $\mathbf{x}(t)$ from leaving $\mathcal{H}(t)$ between sample times, as illustrated using our case study as follows.

Case Study Part vi (Application of Lemma 3): Suppose the same setup as in Case Study Part iv and suppose that the conditions of Lemma 3 hold. It follows that $h(\sigma, \mathbf{x}(\sigma)) = \kappa(\sigma, \mathbf{x}(\sigma))$, so we can instead compute Δ as a bound on the possible overshoot of κ between time steps. Let $r = \min_{\mathbf{x} \in S(t), \mathbf{i} \in T, \mathbf{u} \in U} \ddot{\kappa}(t, \mathbf{x}, \mathbf{u}, \mathbf{0}) = -0.0262$ (recall that Case Study Part iv assumed $\boldsymbol{\xi} \equiv \mathbf{0}$), which leads to the new bound $\Delta = -\frac{1}{8}T^2r = 1.31(10)^{-4}$. Finally, since Lemma 3 also says that $\ddot{\kappa}(\sigma, \mathbf{x}(\sigma), \mathbf{u}, \boldsymbol{\xi}) \geq -\mu$, and we can show that $\min_{\mathbf{x} \in S(t), \mathbf{i} \in T, \mathbf{u} \in U} \ddot{\kappa}(t, \mathbf{x}, \mathbf{u}, \mathbf{0}) = -0.0062$, it follows that $\ddot{\kappa}(t, \mathbf{x}(t), \mathbf{u}, \mathbf{0}) \geq r = -\mu - 0.0062T = -0.00291$ for all $t \in [t_k, t_{k+1}]$ assuming $\sigma \in [t_k, t_{k+1}]$, which leads to $\Delta = -\frac{1}{8}T^2r = 1.46(10)^{-5}$. Thus, Lemma 3 reduces the conservatism Δ on \mathcal{H} needed to ensure safety during the between-sample interval compared to Case Study Part iv.

We now apply Lemma 3 to calculate a general formula for appropriate margins Δ , δ in Eqs. (16) and (17) on $h(t_k, \mathbf{x}_k)$, $\kappa(t_k, \mathbf{x}_k)$ to ensure that \mathbf{x} remains safe between sampling times.

Theorem 1: Suppose that κ is thrice differentiable and of relative degree 2 with respect to Eq. (1), and \boldsymbol{u} is constant on $[t_k, t_{k+1})$. Suppose that all maximizers σ of h in Eq. (13) on the interval (t_k, t_{k+1}) satisfy $\dot{\kappa}(\sigma, \boldsymbol{x}(\sigma)) = 0$. Define δ_1 as

$$\begin{split} \delta_1 &\triangleq \max_{\tau \in [0,T]} \left[\min \left\{ \frac{1}{2} (\mu + M_2^+ - M_2^-) (T - \tau)^2 - \frac{1}{6} M_3^- (T - \tau)^3, \right. \\ &\left. \frac{1}{2} (\mu + M_2^+ - M_2^-) \tau^2 + \frac{1}{6} M_3^+ \tau^3 \right\} \right] \end{split} \tag{24}$$

If $\mathbf{x}(t_k) \in \mathcal{H}^{\delta_1}(t_k) \cap \mathcal{Q}(t_k)$ in Eqs. (16) and (3) and $\mathbf{x}(t_{k+1}) \in \mathcal{H}(t_{k+1}) \cap \mathcal{Q}^{\delta_1}(t_{k+1})$ in Eqs. (10) and (17), then $\mathbf{x}(t) \in \mathcal{H}(t)$ for all $t \in [t_k, t_{k+1}]$.

Case Study Part vii (Application of Theorem 1): Using the values of M_2^- , M_2^+ , M_3^- , M_3^+ , μ in Table 2, it follows that $\delta_1 = 1.10(10)^{-5}$ in Eq. (24). This is of similar magnitude to the value of Δ in Case Study Part vi, as expected, and is equivalent to 2.27 arcseconds of shrinkage of the inner constraint set.

Thus, in the case where the maximizers of κ and h are consistent, we have an explicit formula for how much we should further restrict the set \mathcal{H} at the sample times to ensure that the state never leaves the set \mathcal{H} between the sample times. Having established this, we note that the requirements of Theorem 1 are still overly conservative. This is because we assumed that \mathcal{H}^{Δ} and \mathcal{Q}^{δ} were defined using the same margin parameter $\Delta = \delta = \delta_1$. For certain systems, applying different margins Δ_2 on $h(t_k, x_k)$ and δ_2 on $\kappa(t_k, x_k)$ may reduce this margin, as presented in the following theorem.

Theorem 2: Suppose that κ is thrice differentiable and of relative degree 2 with respect to Eq. (1), and \boldsymbol{u} is constant on $[t_k, t_{k+1})$. Suppose that all maximizers σ of h in Eq. (13) on the interval (t_k, t_{k+1}) satisfy $\dot{\kappa}(\sigma, \boldsymbol{x}(\sigma)) = 0$. Suppose that there exist constants $\delta_2 \geq 0$ and $\Delta_2 \geq 0$ for which it holds that

$$\max_{\tau \in [0,T]} \left[\min \left\{ -\Delta_2 + \frac{1}{2} (\mu + M_2^+ - M_2^-) (T - \tau)^2 - \frac{1}{6} M_3^- (T - \tau)^3, -\delta_2 + \frac{1}{2} (\mu + M_2^+ - M_2^-) \tau^2 + \frac{1}{6} M_3^+ \tau^3 \right\} \right] \le 0$$
 (25)

If $x(t_k) \in \mathcal{H}^{\Delta_2}(t_k) \cap \mathcal{Q}(t_k)$ in Eqs. (16) and (3) and $x(t_{k+1}) \in \mathcal{H}^{\Delta_2}(t_{k+1}) \cap \mathcal{Q}^{\delta_2}(t_{k+1})$ in Eqs. (16) and (17), then $x(t) \in \mathcal{H}(t)$ in Eq. (10) for all $t \in [t_k, t_{k+1}]$.

The primary difference between Theorem 1 and Theorem 2 is that, in Theorem 1, the form for δ_1 was provided explicitly. On the other hand, in Theorem 2, neither δ_2 nor Δ_2 is uniquely defined. If we fix either δ_2 or Δ_2 , we can use condition (25) to compute the other constant. It follows from Theorem 1 that one valid combination is $\Delta_2 = \delta_2 = \delta_1$. Another helpful strategy is to set $\Delta_2 = \Delta_3$, where Δ_3 is presented in the next subsection, and to then compute the smallest allowable δ_2 . We also note that, unlike Theorem 1, the conditions of Theorem 2 are recursively feasible. That is, the ending condition $x(t_{k+1}) \in \mathcal{H}^{\Delta_2}(t_{k+1}) \cap \mathcal{Q}^{\delta_2}(t_{k+1})$ at time t_{k+1} implies the starting condition $x(t_k) \in \mathcal{H}^{\Delta_2}(t_k) \cap \mathcal{Q}(t_k)$ when k advances by one step.

Case Study Part viii (Application of Theorem 2): Using the values of M_2^- , M_2^+ , M_3^- , M_3^+ , μ in Table 2, one possible combination satisfying Eq. (25) besides $\Delta_2 = \delta_2 = \delta_1$ is $\Delta_2 = 1.3(10)^{-5}$ and $\delta_2 = 9.7(10)^{-6}$.

D. Determining Δ , δ When h and κ Have Distinct Maximizers

Now that we have thoroughly covered excursions outside the sets \mathcal{H}^{Δ} , \mathcal{Q}^{δ} when Lemma 3 applies, we finally discuss the behavior between sampling times when this is not the case, as is illustrated by the green lines in Fig. 4.

Lemma 4: Suppose that κ is thrice differentiable and of relative degree 2 with respect to Eq. (1), and \boldsymbol{u} is constant on $[t_k, t_{k+1})$, where $t_{k+1} = t_k + T$. Suppose that $M_3^+ > 0$, $M_3^- < 0$, and $\mu \ge M_2^+ - M_2^- + (\max\{|M_3^+|, |M_3^-|\})T$. Define Δ_3 as in Eq. (A34) in the Appendix. Suppose that there exists a maximizer time $\sigma \in (t_k, t_{k+1})$ for which $h(\sigma, \boldsymbol{x}(\sigma)) \ge h(t, \boldsymbol{x}(t))$ for all $t \in [t_k, t_{k+1}]$ at which $\kappa(\sigma, \boldsymbol{x}(\sigma)) \ne 0$. If $\boldsymbol{x}(t_k) \in \mathcal{H}^{\Delta_3}(t_k) \cap \mathcal{Q}(t_k)$ and $\boldsymbol{x}(t_{k+1}) \in \mathcal{H}^{\Delta_3}(t_{k+1}) \cap \mathcal{Q}(t_{k+1})$, then $\boldsymbol{x}(t) \in \mathcal{Q}(t)$ for all $t \in [t_k, t_{k+1}]$. Moreover, if there exists a time $t_s \in (t_k, t_{k+1})$ at which $\kappa(t_s, \boldsymbol{x}(t_s)) = 0$, then t_s is unique.

Note that in Lemmas 3 and 4, we supposed existence of a local maximizer of h. If a local maximizer of h does not occur on $[t_k, t_{k+1}]$, then it is trivial to show that $x(t) \in \mathcal{H}(t)$ for all $t \in [t_k, t_{k+1}]$, and thus by Lemma 2, $x(t) \in \mathcal{Q}(t)$ for all $t \in [t_k, t_{k+1}]$. Also, it should be emphasized that Lemma 4 does not guarantee that $x(t) \in \mathcal{H}(t)$ for all $t \in [t_k, t_{k+1}]$ as in Theorems 1 and 2, because the value of Δ_3 required to guarantee that result could be larger. Rather, Lemma 4 only guarantees that x(t) stays in the original constraint set $\mathcal{Q}(t)$ for all $t \in [t_k, t_{k+1}]$, and the proof further shows that x(t) stays in $\mathcal{H}(t)$ in the special case where a local maximizer $t_s \in (t_k, t_{k+1})$ of κ also exists.

Case Study Part ix (Application of Lemma 4): Using the values of $M_2^-, M_2^+, M_3^-, M_3^+, \mu$ in Table 2, it follows that $\Delta_3 = 1.09(10)^{-5}$ in Eq. (A34). This occurs for $\gamma = 3.6(10)^{-6}$, $\sigma - t_k = 0.13$ s, and $t_s - \sigma = 0.0023$ s. In this case, $\Delta_3 < \delta_1$, but this is not guaranteed in general.

Remark 1: Note that the necessary condition $\ddot{\kappa}(\sigma, \mathbf{x}(\sigma), \mathbf{u}, \mathbf{\xi}) = -\mu$ in the proof of Lemma 4 [preceding Eq. (A16)] is very specific, so in the authors' experience, maximizers of h meeting the conditions of Lemma 4 are rarer than maximizers meeting the conditions of Lemma 3. However, the conditions of Lemma 4 occur more frequently if μ is chosen very small.

Thus, we have now identified bounds on the overshoot of κ between time steps both when κ and h share maximizers (Lemma 3) and when the maximizer of κ is distinct from the maximizer of h

(Lemma 4). We thus have all the tools we need to define the robust inner constraint set \mathcal{Z} . We now combine Theorem 2 and Lemma 4 to state our main theorem.

Theorem 3: Suppose that κ is thrice differentiable and of relative degree 2 with respect to Eq. (1), and \boldsymbol{u} is constant on $[t_k, t_{k+1})$, where $t_{k+1} = t_k + T$. Suppose that $M_3^+ > 0$, $M_3^- < 0$, and $\mu \ge M_2^+ - M_2^- + \max\{|M_3^+|, |M_3^-|\}T$. Suppose that there exist δ_2 and δ_2 satisfying condition (25), and that $\delta_2 \ge \delta_3$ in Eq. (A34). If $\boldsymbol{x}(t_k) \in \mathcal{H}^{\delta_2}(t_k) \cap \mathcal{Q}(t_k)$ and $\boldsymbol{x}(t_{k+1}) \in \mathcal{H}^{\delta_2}(t_{k+1}) \cap \mathcal{Q}^{\delta_2}(t_{k+1})$, then $\boldsymbol{x}(t) \in \mathcal{Q}(t)$ for all $t \in [t_k, t_{k+1}]$.

It follows from Theorem 3 that we can express the robust inner constraint set as in Fig. 2 as

$$\mathcal{Z}(t_k) = \mathcal{Q}^{\delta_2}(t_k) \cap \mathcal{H}^{\Delta_2}(t_k) \cap \mathcal{H}^{\Delta_3}(t_k)$$
 (26)

Remark 2: Note that δ_1 in Eq. (24) decreases with decreasing μ , while Δ_3 in Eq. (A34) tends to increase with decreasing μ . Although μ is a tunable variable, this tradeoff suggests that there is some minimum amount of margin required when using a ZOH controller, regardless of the choice of μ . Note that both δ_1 and Δ_3 decrease with decreasing T.

E. Determining the Set of Safe Controls

Now that we have thoroughly addressed the problem of overshoot between time steps, we seek a condition on \boldsymbol{u} that guarantees $h(t_{k+1}, \boldsymbol{x}(t_{k+1})) \leq -\Delta_2$ and $\kappa(t_{k+1}, \boldsymbol{x}(t_{k+1})) \leq -\delta_2$ so that we may apply Theorem 3. Moreover, we seek a choice of parameters δ_2 , Δ_2 , μ such that this condition is always feasible with respect to the input constraints everywhere in \mathcal{Z} in Eq. (26). To this end, define the following polynomials in τ :

$$p_{\kappa}(t, \mathbf{x}(t), \mathbf{u}(t), \tau) \triangleq \kappa(t, \mathbf{x}(t)) + \dot{\kappa}(t, \mathbf{x}(t))\tau + \frac{1}{2}\psi(t, \mathbf{x}(t), \mathbf{u}(t))\tau^{2} + \frac{1}{2}M_{2}^{+}\tau^{2} + \frac{1}{6}M_{3}^{+}\tau^{3}$$
(27)

$$p_{h}(t, \boldsymbol{x}(t), \boldsymbol{u}(t), \tau) \triangleq p_{\kappa}(t, \boldsymbol{x}(t), \boldsymbol{u}(t), \tau) + \frac{1}{2\mu} \operatorname{ssq} \left(\dot{\kappa}(t, \boldsymbol{x}(t)) + \psi(t, \boldsymbol{x}(t), \boldsymbol{u}(t)) \tau + M_{2}^{+} \tau + \frac{1}{2} M_{3}^{+} \tau^{2} \right)$$
(28)

which we will show represent upper bounds on $\kappa(t + \tau, \mathbf{x}(t + \tau))$ and $h(t + \tau, \mathbf{x}(t + \tau))$, respectively, given $\mathbf{x}(t)$ and a ZOH $\mathbf{u}(t)$. Here, $\operatorname{ssq}(\lambda) \triangleq \lambda |\lambda|$ for brevity.

Theorem 4: Suppose that κ is thrice differentiable and of relative degree 2 with respect to Eq. (1); $M_3^-, M_3^+, \delta_2, \Delta_2, \Delta_3, \mu$ satisfy the conditions of Theorem 3; \mathcal{Z} is as given in Eq. (26); and \boldsymbol{u} satisfies Eq. (14) for every $k \in \mathbb{N}$. If $\boldsymbol{x}(t_0) \in \mathcal{Z}(t_0)$ and

$$p_{\kappa}(t_k, \mathbf{x}(t_k), \mathbf{u}(t_k, \mathbf{x}(t_k)), T) \le -\delta_2 \tag{29a}$$

$$p_h(t_k, \mathbf{x}(t_k), \mathbf{u}(t_k, \mathbf{x}(t_k)), T) \le -\Delta_2$$
 (29b)

both hold for every $k \in \mathbb{N}$, then $x(t) \in \mathcal{Q}(t)$ for all $t \in \mathbb{T}$.

Note that while the upper bounds p_{κ} and p_h are valid for any $\tau \ge 0$, Theorem 4 only considers the values of p_{κ} and p_h at $\tau = T$, and thus relies on the analysis leading up to Theorem 3 (which was not dependent on p_{κ} , p_h) to guarantee that κ remains nonpositive between sampling times, i.e., for $\tau \in (0, T)$. Based on Theorem 4, we conclude with the following definition of a CBF for ZOH applications, analogous to that in [35] (Def. 2).

Definition 2: For a thrice continuously differentiable constraint function κ_i , the function $h_i: \mathbb{T} \times \mathbb{X} \to \mathbb{R}$ in Eq. (13) with parameter μ is a degree-2 ZOH CBF (D₂ZohCBF) on the set \mathcal{S} for time-step T if there exist constants δ_2 , Δ_2 satisfying Eq. (25) and $\Delta_2 \geq \Delta_3$ in Eq. (A34) such that

$$\min_{\boldsymbol{u}\in\mathcal{U}}(\max\{p_{\kappa_i}(t,\boldsymbol{x},\boldsymbol{u},T)+\delta_2,p_{h_i}(t,\boldsymbol{x},\boldsymbol{u},T)+\Delta_2\})\leq 0,$$

$$\forall x \in \mathcal{Z}_i(t) \cap \mathcal{S}(t), \ \forall t \in \mathbb{T}$$
 (30)

where \mathcal{Z}_i , p_{κ_i} , and p_{h_i} are given in Eqs. (26–28), respectively.

We revert to using the i indexing notation in Definition 2 for completeness (recall that this entire section and thus Definition 2 too are for one constraint at a time). Similar to Eq. (9) with continuous control, Eq. (30) accounts for the allowable control set \mathcal{U} , so if h is a D₂ZohCBF, then the conditions (29) are feasible in the presence of input constraints for all $x(t) \in \mathcal{Z}(t), t \in \mathbb{T}$. Equivalently, if h is a D₂ZohCBF then the set $\mathcal{U}_z(t,x) \cap \mathcal{U}$ is nonempty for all $x \in \mathcal{Z}(t) \cap \mathcal{S}(t), t \in \mathbb{T}$, where

$$\mathcal{U}_z(t, \mathbf{x}) = \{ \mathbf{u} \in \mathbb{R}^m | p_\kappa(t, \mathbf{x}, \mathbf{u}, T) \le -\delta_2 \text{ and } p_h(t, \mathbf{x}, \mathbf{u}, T) \le -\Delta_2 \}$$
(31)

The only remaining component is to determine a valid triple $(\delta_2, \Delta_2, \mu)$. One such triple is $\delta_2 = \delta_1$ in Eq. (24), $\Delta_2 = \Delta_1$ where $\Delta_1 \triangleq \max\{\delta_1, \Delta_3\}$ in Eqs. (24) and (A34), and $\mu = \mu^*$ as follows:

$$\mu^*(\delta_2, \Delta_2) \triangleq \max_{\mu \in (0, \infty)} \mu$$
 such that

$$\max_{\boldsymbol{x} \in \mathcal{Z}(t) \cap S(t) \atop t \in \mathbb{T}} \left(\min_{\boldsymbol{u} \in \mathcal{U}} (\max\{p_{\kappa}(t, \boldsymbol{x}, \boldsymbol{u}, T) + \delta_2, p_{h}(t, \boldsymbol{x}, \boldsymbol{u}, T) + \Delta_2\}) \right) \leq 0$$
(32)

assuming that μ^* exists. One can also choose $\mu \leq \mu^*(\delta_2, \Delta_2)$. Note that for large ξ or T, δ_2 and Δ_2 will also be large, and there may be no μ^* satisfying Eq. (32) and the conditions of Theorem 3, indicating that Eq. (1) cannot be safely controlled at such a sampling time T. A plot of μ^* using $\delta_2 = \delta_1$ and $\Delta_2 = \Delta_1$ for dynamics (2) is shown in Fig. 5, where the black region is where μ^* does not exist or is less than $M_2^+ - M_2^- + \max\{|M_3^+|, |M_3^-|\}T$.

Case Study Part x (Selection of μ for Input Constraints): Using the values of M_2^- , M_2^+ , M_3^- , M_3^+ in Table 2, the choice $(\delta_1, \delta_1, \mu^*(\delta_1, \delta_1))$ where $\mu^*(\delta_1, \delta_1) = 0.00167$ as in Eq. (32) is one valid triple. Alternatively, $(\delta_2, \Delta_2, \mu^*(\delta_2, \Delta_2))$ is another such triple. We note that $\mu^*(\delta_2, \Delta_2)$ is slightly larger than $\mu^*(\delta_1, \delta_1)$, but the difference is only in the fourth significant digit of μ for this particular system. The authors observed a greater difference between $\mu^*(\delta_2, \Delta_2)$ and $\mu^*(\delta_1, \delta_1)$ for problems where u_{\max} was greater. Thus, ZOH discretization has led to a more conservative result than the continuous-time case with $\mu=0.0025$ in Case Study Part iii.

Note that the polynomial p_{κ} is linear in ψ , and therefore affine in u, so one can encode Eq. (29a) in a QP-based control law as in [35] (Sec. II-C). The polynomial p_h has nonlinear dependence on ψ (because of the ssq function), but p_h is still monotone increasing in ψ ,

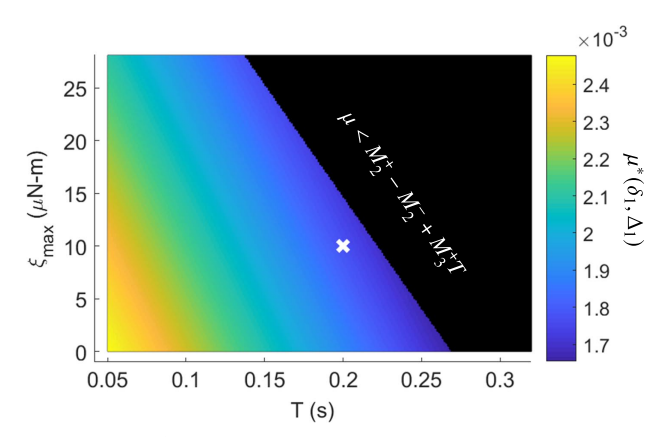


Fig. 5 Plot of μ^* in Eq. (32) variation with the disturbance bound $\xi_{\rm max}$ and sampling period T for the system (2), where "x" marks the case study parameters.

and thus one can write $p_h \leq -\Delta_2$ in Eq. (29b) equivalently as $\psi \leq \psi_{\max}$ for some number ψ_{\max} (the expression for ψ_{\max} is omitted for brevity, but the interested reader is referred to the function get_PhiQ in the simulation code in Sec. V). Thus, one can also encode Eq. (29b) in a QP, and the set \mathcal{U}_z in Eq. (31) is a polytope. In conclusion, the sets \mathcal{Z} in Eq. (26) and \mathcal{U}_z in Eq. (31) solve the relative-degree-2 case of Problem 1.

IV. Method for Relative Degree 1

A. Preliminary Method

We now extend the method in Sec. III to constraint functions that are of relative degree 1 with respect to the dynamics (1). As before, we drop the subscript i and assume that η represents any relative-degree-1 constraint function. In this section, we assume that η is also a CBF, so we will not need to employ the intermediary step of defining h and \mathcal{H} , as was done for relative-degree-2 constraints. Similar to Eq. (19), define the function

$$\phi(t, \mathbf{x}, \mathbf{u}) \triangleq \frac{\partial \eta(t, \mathbf{x})}{\partial t} + \frac{\partial \eta(t, \mathbf{x})}{\partial \mathbf{v}} f_2(t, \mathbf{x}) + g_1(t, \mathbf{x})\mathbf{u}$$
(33)

which represents the component of $\dot{\eta}$ that is known to the controller. Likewise, define the constant

$$M_1 \triangleq \sup_{t \in \mathbb{T}, \mathbf{x} \in S(t)} \underbrace{\frac{\partial \eta(t, \mathbf{x})}{\partial \mathbf{v}}} g_2(t, \mathbf{x}) \boldsymbol{\xi}$$
(34)

which represents our uncertainty in $\dot{\eta}$ because of the unknown disturbance. It then holds that

$$\dot{\eta}(t, \mathbf{x}, \mathbf{u}) \le \phi(t, \mathbf{x}, \mathbf{u}) + M_1 \tag{35}$$

Because we intend to implement a ZOH controller, we then define

$$M_{2} \triangleq \sup_{t \in \mathbb{T}, \mathbf{x} \in \mathcal{S}(t), \mathbf{u} \in \mathcal{U}, \boldsymbol{\xi} \in \Xi} \left[\frac{\partial \phi(t, \mathbf{x}, \mathbf{u})}{\partial t} + \frac{\partial \phi(t, \mathbf{x}, \mathbf{u})}{\partial q} f_{1}(t, \mathbf{x}) \right. \\ \left. + \frac{\partial \phi(t, \mathbf{x}, \mathbf{u})}{\partial \mathbf{v}} (f_{2}(t, \mathbf{x}) + g_{1}(t, \mathbf{x})\mathbf{u} + g_{2}(t, \mathbf{x})\boldsymbol{\xi}) \right]$$
(36)

so that for $\tau \geq 0$ it holds that

$$\phi(t+\tau, \mathbf{x}(t+\tau), \mathbf{u}) \le \phi(t, \mathbf{x}(t), \mathbf{u}) + M_2 \tau \tag{37}$$

In this section, we only require the upper bounds on Eqs. (34) and (36), so we omit the superscripts + and - used in the prior section. Here, M_1 and M_2 are analogous to M_2^+ and M_3^+ , respectively, from Sec. III.B. Now define the following polynomial in τ

$$p_{\eta}(t, \mathbf{x}, \mathbf{u}, \tau) \triangleq \eta(t, \mathbf{x}) + \phi(t, \mathbf{x}, \mathbf{u})\tau + M_1 \tau + \frac{1}{2} M_2 \tau^2$$
 (38)

which serves as an upper bound on the evolution of η and is employed in the following theorem.

Theorem 5: Suppose that η is twice differentiable and of relative degree 1 with respect to Eq. (1) and \boldsymbol{u} satisfies Eq. (14) for every $k \in \mathbb{N}$. Suppose that $M_2 \geq 0$ in Eq. (36). If $\boldsymbol{x}(t_0) \in \mathcal{V}(t_0)$ and

$$p_n(t_k, \mathbf{x}(t_k), \mathbf{u}(t_k, \mathbf{x}(t_k)), T) \le 0$$
 (39)

for every $k \in \mathbb{N}$, then $x(t) \in \mathcal{V}(t)$ for all $t \in \mathbb{T}$.

Note that Theorem 5 is a straightforward extension of [29] (Cor. 3) to systems with disturbances, while the insights in the following subsection are new to this paper and motivated specifically by the system in Eq. (2).

Case Study Part xi (Application of Theorem 5): For the system (2), in order for the constants $M_2^-, M_2^+, M_3^-, M_3^+$ for κ_b in Eq. (5) to be well-defined [i.e., for S in Eqs. (18) and (21) to be compact], the maximum system angular velocity must be bounded. There are various ways to encode such a bound. First, if one desires that

 $\|\omega\| \le \omega_{\max}$ for some $\omega_{\max} \in \mathbb{R}_{>0}$, then one could use either $\eta_1(t, \mathbf{x}) = \|\omega\| - \omega_{\max}$ or $\eta_2(t, \mathbf{x}) = \|\omega\|^2 - \omega_{\max}^2$. Note that M_2 is undefined for the constraint function η_1 , so Theorem 5 does not apply. Instead, suppose that we choose η_2 . Then, letting $\omega_{\max} = 0.0175$ rad/s, it follows that $M_2 = 0.00153$. While η_2 satisfies the definition of $D_1\mathrm{ZohCBF}$, this leads to an effective margin of $(\frac{1}{2}M_2T^2)/w_{\max}^2 \approx 10\%$, which is rather large. While this does not directly impact the robust inner constraint set Z in Eq. (46), this margin in effect makes certain states in the safe set inaccessible (see [29] for a more extensive discussion of ZOH margins), so we would like to reduce this margin

Next, suppose that the matrix Z in Eq. (2) is of the form

$$Z = \begin{bmatrix} Z_{11} & Z_{12} \\ Z_{21} & Z_{22} \end{bmatrix} \tag{40}$$

where $Z_{11} \in \mathbb{R}^{3\times 3}$, $Z_{12} \in \mathbb{R}^{3\times m}$, $Z_{21} \in \mathbb{R}^{m\times 3}$, $Z_{22} \in \mathbb{R}^{m\times m}$. Note that, under the dynamics in Eq. (2), $\|\omega\|^2$ is not a conserved quantity, so if the spacecraft is not spinning about a principal axis, it will take active control effort to keep the state within a level set of η_2 . On the other hand, kinetic energy is a conserved quantity, which takes no control effort to maintain (unless the disturbance adds energy to the system). For this reason, define P in η_{ω} in Eq. (7) as $P = Z_{11}^{-1}$, so that η_{ω} encodes a maximum kinetic energy constraint. Then, using η_{ω} in Eq. (7) with e_{\max} in Table 1, one finds $M_2 = 8.30(10)^{-5}$, leading to a smaller effective margin of $(\frac{1}{2}M_2T^2)/e_{\max} \approx 3.3\%$.

B. Reducing Conservatism

Before we present a definition for a valid CBF for the relative-degree-1 case, we present an extension of Theorem 5 that reduces conservatism for certain systems and constraint functions, and in particular the constraint function η_{ω} in our case study in Eq. (7). In developing this paper, the authors noticed that the main contributor to M_2 for the constraint function in Eq. (7) was the control input \boldsymbol{u} . While \boldsymbol{x} and $\boldsymbol{\xi}$ are not known exactly between time steps t_k and t_{k+1} , the value of $\boldsymbol{u}(t) = \boldsymbol{u}(t_k)$ for $t \in (t_k, t_{k+1})$ is a known quantity, and thus can be removed from the uncertainty bound M_2 . Motivated by this, suppose that there exists functions $\phi_1: \mathcal{U} \to \mathbb{R}_{\geq 0}$ and $\phi_2: \mathbb{T} \times \mathcal{S} \times \mathcal{U} \times \Xi \to \mathbb{R}$ such that

$$\dot{\phi}(t, \mathbf{x}, \mathbf{u}, \boldsymbol{\xi}) \equiv \phi_1(\mathbf{u}) + \phi_2(t, \mathbf{x}, \mathbf{u}, \boldsymbol{\xi}) \tag{41}$$

for all $t \in \mathbb{T}$, $x \in \mathcal{S}$, $u \in \mathcal{U}$, $\xi \in \Xi$. The value of $\phi_1(u)$ is known, so define a constant analogous to Eq. (36) using ϕ_2 only as

$$M_2^{\text{alt}} \triangleq \sup_{t \in \mathbb{T}. x \in \mathcal{S}(t). u \in \mathcal{U}. \xi \in \Xi} \phi_2(t, x, u, \xi)$$
 (42)

Then we can define the polynomial

$$p_{\eta}^{\text{alt}}(t, \mathbf{x}, \mathbf{u}, \tau) \triangleq \eta(t, \mathbf{x}) + \phi(t, \mathbf{x}, \mathbf{u})\tau + M_1\tau + \frac{1}{2}\left(\phi_1(\mathbf{u}) + M_2^{\text{alt}}\right)\tau^2$$
(43)

Corollary 1: Suppose that η is twice differentiable and of relative degree 1 with respect to Eq. (1) and \boldsymbol{u} satisfies Eq. (14) for all $k \in \mathbb{N}$. Suppose that ϕ_1 in Eq. (41) is positive semidefinite and $M_2^{\text{alt}} \geq 0$ in Eq. (42). If $\boldsymbol{x}(t_0) \in \mathcal{V}(t_0)$ and

$$p_n^{\text{alt}}(t_k, \mathbf{x}(t_k), \mathbf{u}(t_k, \mathbf{x}(t_k)), T) \le 0$$
 (44)

for every $k \in \mathbb{N}$, then $x(t) \in \mathcal{V}(t)$ for all $t \in \mathbb{T}$.

We are now ready to give the complete requirements for a relative-degree-1 constraint function η to be a CBF in ZOH applications.

Definition 3: A twice continuously differentiable function η_i is a degree-1 ZOH CBF (D₁ZohCBF) on the set \mathcal{S} for time-step T if there exists a positive semidefinite function $\phi_1: \mathcal{U} \to \mathbb{R}_{\geq 0}$ and a function $\phi_2: \mathbb{T} \times \mathcal{S} \times \mathcal{U} \times \Xi$ (where one can use $\phi_1(u) \equiv 0$) satisfying Eq. (41) such that

$$\min_{\boldsymbol{u} \in \mathcal{I}_{\ell}} p_{\eta_{i}}^{\text{alt}}(t, \boldsymbol{x}, \boldsymbol{u}, T) \leq 0, \quad \forall \boldsymbol{x} \in \mathcal{S}(t), \ \forall t \in \mathbb{T}$$
 (45)

where $p_{n_i}^{\text{alt}}$ is as given in Eq. (43).

That is, η is a D₁ZohCBF if the condition (39) is always feasible inside the safe set. Unlike Definition 2, Definition 3 does not contain any additional tuning parameters. We assume that the function η has already been constructed or tuned so as to be possible to render the corresponding set ${\mathcal V}$ forward invariant in the presence of input constraints. This is reasonable in the context of spacecraft attitude control, because the function η_{ω} in Eq. (7) represents spacecraft kinetic energy. A fundamental requirement of control design should be that the spacecraft is able to reduce its kinetic energy from any safe state. In math, this requirement is equivalent to Eq. (45) for η_{ω} . One case in which this requirement is not satisfied is if the spacecraft is allowed to achieve large angular velocities while operating at a control frequency too slow to stabilize the system. In this case, no amount of tuning will yield a safe controller, so Eq. (45) will be violated, and one will need to operate at lower angular velocities or smaller time steps to achieve a stable system and satisfy Eq. (45).

For the D₁ZohCBF, denote

$$\mathcal{Z}(t) \equiv \mathcal{V}(t), \quad \mathcal{U}_z(t, \mathbf{x}) = \{ \mathbf{u} \in \mathbb{R}^m | p_n^{\text{alt}}(t, \mathbf{x}, \mathbf{u}, T) \le 0 \}$$
 (46)

which solves the relative-degree-1 case of Problem 1. Note that if $\phi_1 \equiv 0$ in Eq. (41), then \mathcal{U}_z in Eq. (46) is a half-space and safe control inputs can again be computed using a QP-based control law. Alternatively, if ϕ_1 is a convex function, then \mathcal{U}_z in Eq. (46) is not necessarily a polytope, but will still be a convex set, allowing the use of other convex optimization tools to choose control inputs. For instance, in Sec. V.A, ϕ_1 will be a strictly convex quadratic function, yielding a quadratically constrained quadratic program (QCQP) as a control law.

Case Study Part xii (Application of Corollary 1): Suppose that η_2 is as described in Case Study Part xi, and let $\phi_1(\mathbf{u}) = 2\mathbf{u}^T Z_{12}^T Z_{12}\mathbf{u}$. This leads to $M_2^{\text{alt}} = 4.88(10)^{-4}$, resulting in an effective margin of $(\frac{1}{2}M_2^{\text{alt}}T^2)/w_{\text{max}}^2 \approx 3.2\%$, much less than in the prior case with $\phi_1(\mathbf{u}) \equiv 0$. Thus, when $\phi_1(\mathbf{u})$ is large, we still end up applying the same amount of margin as in Case Study Part xi, but when $\phi_1(\mathbf{u})$ is small (i.e., \mathbf{u} is small), the margin inherent in p_η^{alt} in Eq. (43) is reduced compared to the margin in p_η in Eq. (38).

Next, for η_{ω} with P as described in Case Study Part xi, let $\phi_1(u) = u^T Z_{12}^T P Z_{12} u$, resulting in $M_2^{\rm alt} = 1.95(10)^{-5}$. This yields an effective margin of $(\frac{1}{2}M_2^{\rm alt}T^2)/e_{\rm max} \approx 0.77\%$, and is therefore the setup used for simulation in Sec. V.A.

V. Simulations

A. Preliminary Simulations

In this section, we demonstrate the above methods in simulation. We assume a spacecraft with two instruments with boresight vectors b_1 , b_2 and keep-out zones θ_1 , θ_2 in Table 3, which induce two pointing constraint functions κ_1 , κ_2 of the form in Eq. (5). Let $s_1 = s_2$ be the local sun vector, which is slowly time-varying. We construct two D₂ZohCBFs h_1 , h_2 as in Sec. III with the constants in Table 2. Suppose that there is also an angular velocity constraint function η_3 of the form in Eq. (7) with the previously presented parameters in Table 1, and with $\phi_1(u) = u^T Z_{12}^T P Z_{12} u$ as discussed in Case Study Part xii. Then η_3 is a D₁ZohCBF. The set of safe control inputs is $\mathcal{U} \cap \mathcal{U}_{z1}(t,x) \cap \mathcal{U}_{z2}(t,x) \cap \mathcal{U}_{z3}(t,x)$.

Suppose that the spacecraft (visualized in Fig. 1) is required to point instrument b_1 at inertially fixed target b_t , given in Table 3. Define the following shortest-path proportional-derivative control law:

$$\varphi = \operatorname{sat}_{\varphi*} \left(\operatorname{arccos} \left(\boldsymbol{b}_{t}^{\mathsf{T}} R(\boldsymbol{q}) \boldsymbol{b}_{1} \right) \right) \tag{47a}$$

$$\mathbf{y} = \mathbf{b}_1 \times \left(R(\mathbf{q})^{\mathrm{T}} \mathbf{b}_t \right) \tag{47b}$$

Table 3 Simulation parameters for Sec. V.A

Parameter	Value
b_1	$[0.5774, 0.5774, 0.5774]^{T}$
\boldsymbol{b}_2	$[-0.8660, 0.5, 0]^{T}$
\boldsymbol{b}_t	$[0, -0.7072, -0.7072]^{T}$
θ_1	$\pi/4$ rad
θ_2	$\pi/4$ rad
φ^*	0.2 rad
k_p	0.1
k_d	0.5
$\boldsymbol{q}(t_0)$	$[0.5, 0.5, 0.5, 0.5]^{\mathrm{T}}$
$\boldsymbol{\omega}(t_0)$	$[0, 0, 0]^{\mathrm{T}}$
$\boldsymbol{w}(t_0)$	$[0, 0, 0, 0]^{\mathrm{T}}$

$$\boldsymbol{u}_{\mathrm{pd}}(t, \boldsymbol{x}) = Z_{12}^{\dagger} \left(k_p \sin \left(\frac{\varphi}{2} \right) \frac{\boldsymbol{y}}{\|\boldsymbol{y}\|} - k_d \boldsymbol{\omega} \right) \tag{47c}$$

where $u_{\rm pd}$ may be unsafe and does not necessarily satisfy the input constraints. Here, let sat be the saturation function and Z_{12}^{\dagger} be the Moore–Penrose pseudoinverse. We then construct the final control law as a QCQP:

$$\mathbf{u}_{\text{zohebf}} = \underset{\mathbf{u} \in \mathcal{U} \cap \mathcal{U}_{z_1}(t, \mathbf{x}) \cap \mathcal{U}_{z_2}(t, \mathbf{x}) \cap \mathcal{U}_{z_3}(t, \mathbf{x})}{\arg \min} \|\mathbf{u} - \mathbf{u}_{\text{pd}}(t, \mathbf{x})\|^2$$
(48)

Using this "ZohCBF" controller, we simulated a single reorientation maneuver with initial and final parameters given in Table 3, and in the presence of a random disturbance bounded by ξ_{max} in Table 1. For

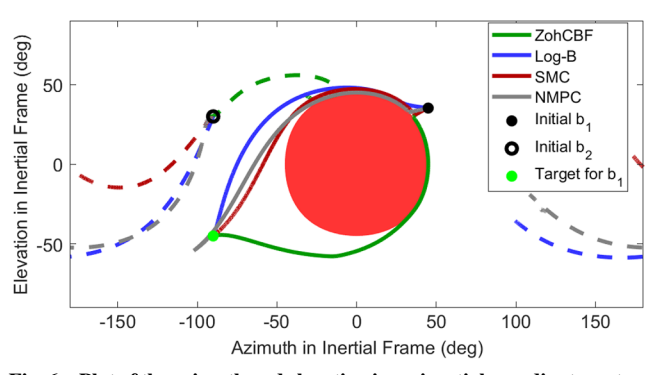


Fig. 6 Plot of the azimuth and elevation in an inertial coordinate system of the two instrument pointing vectors b_1 (solid) and b_2 (dashed) and the keep-out zone (red) centered about the sun vector.

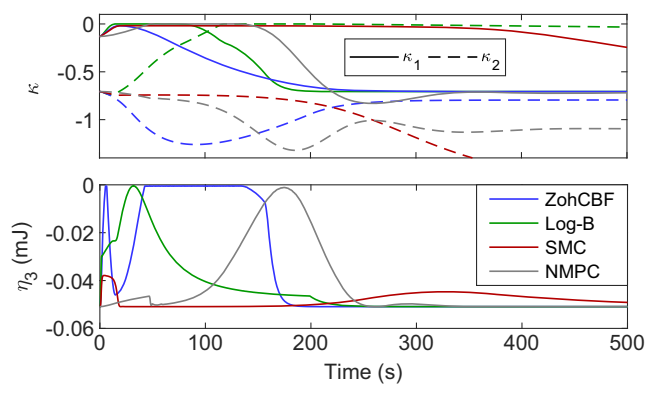


Fig. 7 Plots of the two instrument constraint values κ_1, κ_2 for the lines in Fig. 6, and the system energy constraint values η_3 using all control laws.

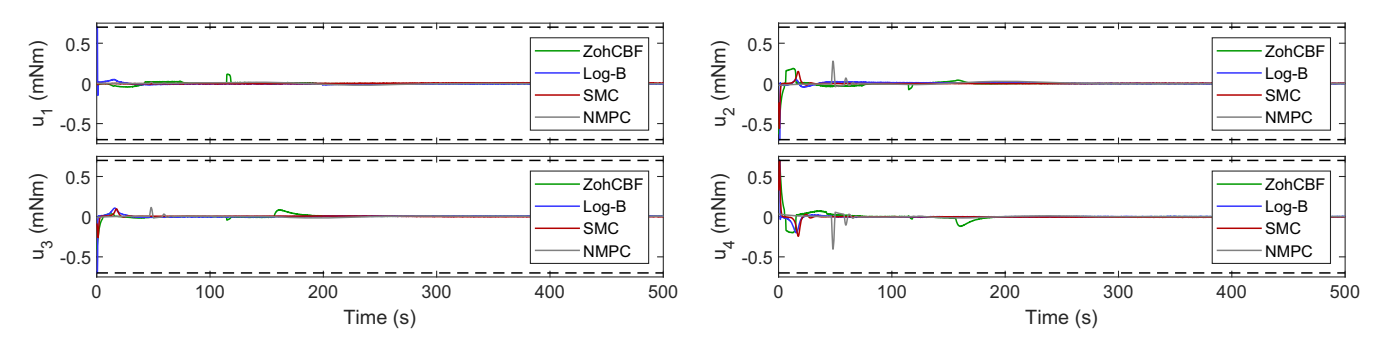


Fig. 8 Plots of the control inputs and input constraints (black dashed lines) for Fig. 6 using all control laws.

Table 4 Simulation times for Figs. 6–8

Method	Settling time, s	Mean compute time, s	Max compute time, s
CBF	207.0	0.0088	0.021
Log-B	338.8	0.00022	0.0082
Log-B SMC	1719.8	0.00016	0.0087
NMPC	803.6	0.15	2.3

more details, we refer the interested reader to the simulation code. The simulation is short enough that we do not presently concern ourselves with momentum management (i.e., ensuring that w_i remains bounded for i=1,2,3,4). A diagram of the excluded pointing zone and the trajectories of the two instrument vectors is shown in Fig. 6, and a video of the reorientation in three dimensions can be found below. The constraint values over the maneuver duration are shown in Fig. 7, and the control inputs are shown in Fig. 8. As expected, safety is maintained, and the control input constraints are always satisfied. The absolute value of the maximum value of η_3 in Fig. 7 is the "controller margin" explained in [29]. Both ZohCBF plots in Fig. 7 exhibit a controller margin, but the margin is only noticeable for the constraint η_3 without zooming in.

For comparison, we also simulated the controllers in 1) [21] (Eq. 22), denoted "Log-B", with $\alpha = 0.75$, $\beta = 8$, $k_1 = 0.0165$; 2) [17] (Eq. 17) denoted "SMC", with k = 0.01, $k_1 = 5015$, $k_2 = 0.0167$, $\bar{d} \equiv 0$; and 3) [12], denoted "NMPC", with n = 5, h = 0.2, $Q_1 = P_1 = 0.01I$, $Q_2 = P_2 = 38I$, $Q_3 = 100I$, where Iis the identity matrix. The resultant trajectories are shown in Figs. 6–8 and described in Table 4, where all simulations were run on a 3.5 GHz Intel Xeon processor. While the Log-B and SMC controllers do not guarantee safety in the presence of input constraints or ZOH control inputs, Figs 6-8 show that when properly tuned, all of the above controllers can behave similarly. That said, the ZohCBF controller took a different route around the exclusion zone than all of the comparison controllers. The ZohCBF and NMPC controllers approached closer to the edge of the safe set than the Log-B and SMC controllers, and the NMPC controller briefly violated the κ_1 constraint. Also, the Lyapunov function introduced in [21] is infinitely differentiable, so the trajectories under the Log-B controller are smooth. We observe this particularly in Fig. 7, where the green lines have unique maximizers, whereas the other controllers spend much of the trajectory very close to zero. This allowed the ZohCBF controller to achieve the fastest settling time, defined here as time to 0.1 deg error, in Table 4. We note that for larger values of k_1 , the Log-B controller could be faster but would exceed the angular velocity constraint, and for much larger values of k_1 , the Log-B controller would violate the pointing constraints due the ZOH implementation. The NMPC controller approached the target at a rate similar to the ZohCBF controller, but exhibited oscillations around the target due to the small prediction horizon, thus resulting in a large settling time.

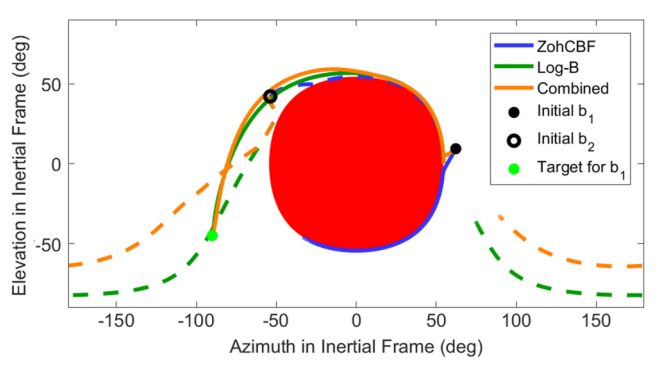


Fig. 9 Plot of the azimuth and elevation in an inertial coordinate system of the two instrument pointing vectors b_1 (solid) and b_2 (dashed) in the presence of a larger exclusion zone than in Fig. 6.

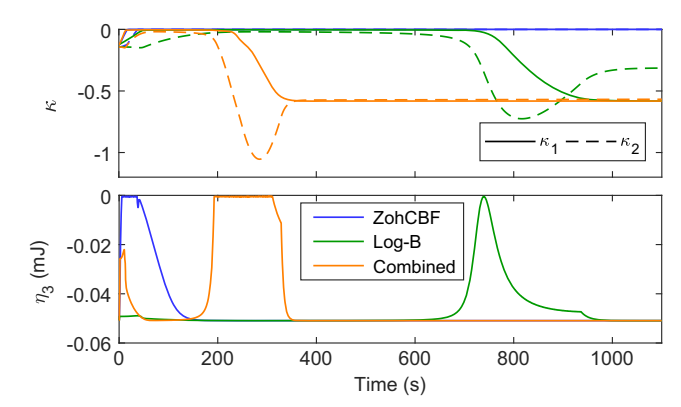


Fig. 10 Plots of the two instrument constraint values κ_1 , κ_2 for the lines in Fig. 9, and the system energy constraint values η_3 using all three control laws.

The SMC controller was the slowest due to the upper bound on k implied by [17] (Eq. 16).

Another notable difference between the ZohCBF and Log-B controllers is that the Lyapunov function in [21] is strictly convex, so the controller is globally convergent. This is not true of the ZohCBF or NMPC controllers. To examine this, we increased the value of θ_1,θ_2 to 0.95 rad and resimulated the ZohCBF and Log-B controllers. The results are shown in Figs. 9 and 10 and Table 5 and are demonstrated in the video below.** Note that the blue lines (ZohCBF controller) in Fig. 9 both approach the edge of the red region, and then stop when the controller cannot safely move closer to the target direction (green dot) due to the set $\mathcal{S} \cap \mathcal{Z}_1 \cap \mathcal{Z}_2 \cap \mathcal{Z}_3$ being nonconvex. The spacecraft remains safe, but does not complete its objective. On the other

[§]All simulation code can be found at https://github.com/jbreeden-um/phd-code/tree/main/2022.

https://youtu.be/EVuyZ-06-1Y.

^{**}https://youtu.be/sZ F4N75kcw.

Table 5 Simulation times for Figs. 9 and 10

Method	Settling time, s	Mean compute time, s	Max compute time, s
CBF	00	0.0072	0.0237
Log-B	1079.6	0.00024	0.0084
Combined	374.2	0.0097	0.0243

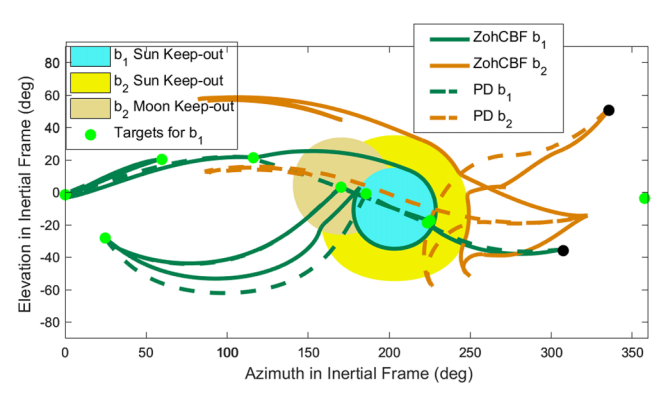


Fig. 11 Plot of the azimuth and elevation in an inertial coordinate system of the instrument pointing vector b_1 (green) and star tracker pointing vector b_2 (orange) along with all three keep-out zones.

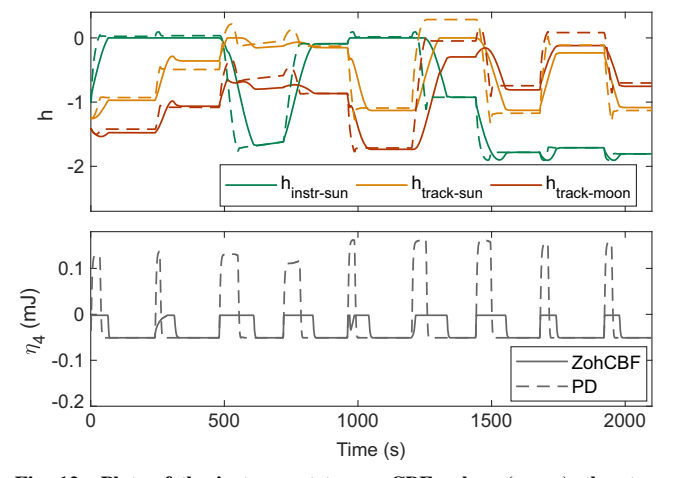


Fig. 12 Plots of the instrument to sun CBF values (green), the star tracker to sun CBF values (orange), and the star tracker to moon CBF values (red) for the lines in Fig. 11, and the system energy constraint (gray) values η_4 using both control laws.

hand, the Log-B controller is eventually able to navigate around the exclusion zone and converge to the target vector. That said, the Log-B controller is very slow in Table 5. Lastly, we note that the ZohCBF technique can be applied to any nominal controller, so we introduce the control law

$$\boldsymbol{u}_{\text{combined}} = \underset{\boldsymbol{u} \in \mathcal{U} \cap \mathcal{U}_{z_1}(t, \boldsymbol{x}) \cap \mathcal{U}_{z_2}(t, \boldsymbol{x}) \cap \mathcal{U}_{z_3}(t, \boldsymbol{x})}{\text{arg min}} \|\boldsymbol{u} - \boldsymbol{u}_{\text{logb-fast}}(t, \boldsymbol{x})\|^2 \quad (49)$$

which we call the "Combined" controller. The controller $u_{logb-fast}$ in Eq. (49) is the same as the Log-B controller, but with a much more aggressive choice of gain $k_1=0.04$. Without the ZohCBF application, the controller $u_{logb-fast}$ would violate the system energy constraint η_3 , but with the additional ZohCBF acting as a safety-filter, the controller $u_{combined}$ yields the orange trajectory in Figs. 9 and 10. Unlike under u_{zohcbf} , the trajectory under $u_{combined}$ converged to the target, and exhibited a reduced settling time in Table 5 compared to the Log-B controller.

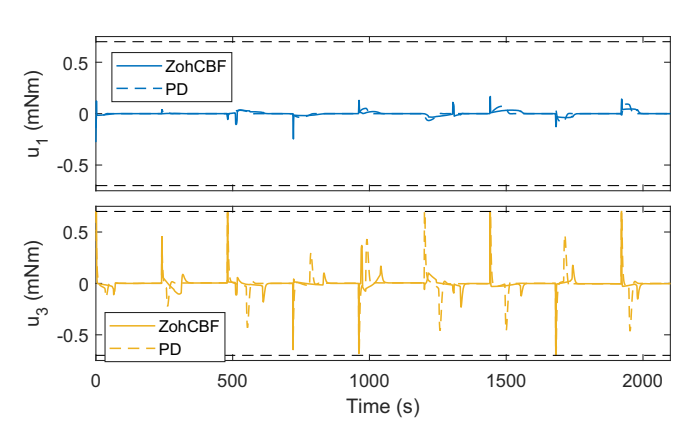
Remark 3: We note that while the controllers (48) and (49) were successful in the simulations above, it still may be possible for the optimizations (48) and (49) to become infeasible because these controllers apply multiple CBFs at once. Progress toward provably guaranteed feasibility of multiple CBFs simultaneously with input constraints is studied in continuous time in [37], and such studies for sampled-data CBFs are left to future work.

B. Spacecraft Simulator Simulations

The prior subsection validates the methods in Secs. III and IV in a simple simulation, so we now present results from a more detailed spacecraft simulator, specifically the NASA "42" open-source spacecraft attitude control simulator [44]. Here, rather than random disturbances, the disturbances are representative of disturbances in the orbital environment for an input spacecraft geometry and specified solar and geomagnetic activity indices.

Specifically, we simulated a 6U CubeSat with the parameters presented in Table 1 in a 500 km altitude circular Earth orbit. Suppose that the spacecraft has a single instrument that must point at a sequence of targets but must avoid the sun by at least 25° (encoded in κ_1), and a star tracker that must not point at the sun within 45° (encoded in κ_2) or the moon within 30° (encoded in κ_3). The angular velocity is constrained by $\eta_4 = \eta_\omega$ as in Case Study Part xi, where we now use $\phi_1(u) = 0$, so that $M_2^{\rm alt} = M_2 = 8.3(10)^{-5}$. This change makes $\mathcal{U}_{z_1} \cap \mathcal{U}_{z_2} \cap \mathcal{U}_{z_3} \cap \mathcal{U}_{z_4}$ a polytope and thus changes Eq. (48) from a QCQP to a regular QP, which was implemented using the fast Operator Splitting QP solver [45]. Finally, the code limited the QP solver to only 20 solver iterations to mimic realistic spacecraft computing constraints. For more details and input parameters, the interested reader is referred to the simulation code.

The instrument and star tracker pointing vectors are shown in Fig. 11, the constraint values are shown in Fig. 12, and the control inputs are shown in Fig. 13 using both u_{zoholf} in Eq. (48) and u_{pd} in



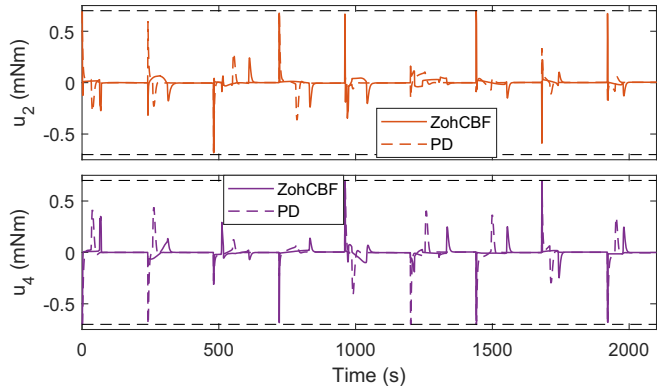


Fig. 13 Plots of the control inputs and input constraints (black dashed lines) for Fig. 11 using both control laws.

Eq. (47c). A video of the reorientation sequence is linked below. †† All constraints and actuator limits were satisfied for the entire pointing sequence using the ZohCBF controller (solid lines in Fig. 11), while there were several constraint violations using the nominal controller (dashed lines in Fig. 11). We note that three of the targets (green dots in Fig. 11) were located very close to the sun vector (i.e., outside the safe set), so the ZohCBF controller prioritized safety over convergence for these targets.

VI. Conclusions

We have presented a methodology for ensuring that trajectories of a dynamic system always remain within a specified constraint set in the presence of ZOH sampled-data control inputs, bounded disturbances, and input constraints using extensions of CBF theory. This methodology is generally applicable to constraint functions of relative degree 1 or 2, and was specialized to spacecraft attitude control. Special attention was devoted to decreasing the margins for overshoot in the case of relative-degree-2 constraints, and for the case of a relative-degree-1 kinetic energy constraint specifically. The methodology was then demonstrated in simulation, where it exhibited faster settling times than all compared online controllers (note that path-planning methods were not tested). While the methods in this paper provably achieve all desired safety criteria, the comparison plots show that similar safe reorientations can be achieved with the comparison methods, although only with careful tuning and without proof of safety under these circumstances. The improvement in convergence by the "combined" controller over the original ZohCBF controller show that this approach may be limited in part by the capabilities of the nominal control law, so choosing "optimal" nominal control laws is one area of future work. Additional future work includes the incorporation of momentum-management techniques and measurement-delay considerations, and study of more general conditions on the existence of a guaranteed safe control input in the presence of several CBFs simultaneously.

Appendix: Proofs

For brevity, we only write out the time argument of κ , η , h, ψ , ϕ , ϕ_1 , p_{κ} , p_h , p_{η} , and p_{η}^{alt} and their derivatives in the following proofs.

Proof of Lemma 3: Note that, on the open interval (t_k, t_{k+1}) , the functions κ , $\dot{\kappa}$, $\ddot{\kappa}$, and $\ddot{\kappa}$ are continuous due to the assumptions on f_1, f_2, g_1, g_2, ξ in Eq. (1) and how \boldsymbol{u} is constant. We divide this proof into two cases depending on whether $\dot{\kappa}$ changes signs at σ .

First, suppose that $\dot{\kappa}$ does not change signs at σ [including the case where $\dot{\kappa}(t) = 0$ for all $t \in (t_k, t_{k+1})$]. This can only occur if $\ddot{\kappa}$ changes signs at σ or if $\ddot{\kappa}(t)$ is zero for all $t \in (t_k, t_{k+1})$. Since $\ddot{\kappa}$ is continuous, this implies $\ddot{\kappa}(\sigma) = 0$. Since $\mu > 0$, it follows that there exists sufficiently small $\tau > 0$ such that $|\ddot{\kappa}(t)| < \mu$ for all t in a neighborhood $t \in (\sigma - \tau, \sigma + \tau)$. Note that \dot{h} is given by

$$\dot{h}(t) = \dot{\kappa}(t) + \frac{1}{\mu} |\dot{\kappa}(t)| \ddot{\kappa}(t) \tag{A1}$$

It follows from Eq. (A1) that $\dot{h}(t)$ has the same sign as $\dot{\kappa}(t)$ for all $t \in (\sigma - \tau, \sigma + \tau)$. Since $\dot{h}(\sigma)$ does not change signs, σ cannot be a local maximizer of h on (t_k, t_{k+1}) unless $\dot{\kappa}(t) = \dot{h}(t) = \ddot{\kappa}(t) = 0$ for all $t \in (t_k, t_{k+1})$, in which case the lemma is trivially true.

Second, suppose that \dot{k} does change signs at σ . The second derivative of h is

$$\ddot{h}(t) = \ddot{\kappa}(t) + \frac{1}{\mu} \operatorname{sign}(\dot{\kappa}(t)) \ddot{\kappa}(t)^2 + \frac{1}{\mu} |\dot{\kappa}(t)| \ddot{\kappa}(t)$$
(A2)

so h is twice differentiable for almost all $t \in [t_k, t_{k+1}]$. Therefore, a necessary condition for σ to be local maximizer of h is for \ddot{h} to be nonpositive in a neighborhood of σ . At $t = \sigma$ exactly, $\ddot{h}(\sigma)$ is unde-

fined since we assumed $\dot{\kappa}(\sigma)$ to be zero, but the limits of $\ddot{h}(t)$ as t approaches σ from the left and right are well-defined and must both be nonpositive for σ to be a maximizer of h. These limits are

$$\ddot{h}^{-}(\sigma) = \lim_{\dot{\kappa}(t) \to 0^{-}} \ddot{h}(t) = \ddot{\kappa}(\sigma) - \frac{\ddot{\kappa}(\sigma)^{2}}{\mu}$$
 (A3a)

$$\ddot{h}^{+}(\sigma) = \lim_{\ddot{\kappa}(t) \to 0^{+}} \ddot{h}(t) = \ddot{\kappa}(\sigma) + \frac{\ddot{\kappa}(\sigma)^{2}}{\mu}$$
 (A3b)

A necessary condition for both Eqs. (A3a) and (A3b) to be non-positive simultaneously is for $0 \ge \ddot{\kappa}(\sigma) \ge -\mu$. Since $\ddot{\kappa}(\sigma) \le 0$, and we assumed $\dot{\kappa}(t)$ changed sign at σ , it follows that σ is necessarily also a maximizer of κ , so the lemma holds in this case as well.

Proof of Theorem 1: The trajectory x(t) belongs to $\mathcal{H}(t)$ for all $t \in [t_k, t_{k+1}]$ if the maximum value $h(\sigma)$ for some maximizer $\sigma \in [t_k, t_{k+1}]$ satisfies $h(\sigma) \leq 0$, so we proceed by trying to bound $h(\sigma)$ using Lemma 3 and the system constants (18) and (21). By assumption, $h(t_k) \leq -\delta_1 \leq 0$ and $h(t_{k+1}) \leq 0$, so the theorem is immediately true in the case where σ is either endpoint. By Lemma 3, if σ is a local maximizer of h on the open interval (t_k, t_{k+1}) , then σ must also be a local maximizer of κ . This implies that $h(\sigma) = \kappa(\sigma)$. Thus, we focus on κ instead of h going forward.

Suppose that there exists a local maximizer σ of κ on (t_k, t_{k+1}) for which $\kappa(\sigma) = h(\sigma) > \max\{h(t_k), h(t_{k+1})\}$. The largest possible value of $\kappa(\sigma)$ occurs when $\dot{\kappa}(t)$ is positive for all $t \in [t_k, \sigma)$ and negative for all $t \in (\sigma, t_{k+1}]$, so without loss of generality, suppose that the sign of $\dot{\kappa}(t)$ follows this partitioning. By assumption, $h(t_k) \leq -\delta_1$, and since we assumed that $\dot{\kappa}(t_k) > 0$, it follows from Eq. (13) that $\kappa(t_k) \leq -\delta_1$ as well. Thus, for the worst-case value of $\kappa(\sigma)$, both $\kappa(t_k)$ and $\kappa(t_{k+1})$ are at most $-\delta_1$. Also, by Lemma 3, $\ddot{\kappa}(\sigma) \geq -\mu$. It follows from Eq. (23a) that

$$\ddot{\kappa}(\sigma + \tau) \ge -\mu + M_2^- + M_3^- \tau - M_2^+ \tag{A4}$$

Thus, we can lower bound $\dot{\kappa}(t)$ for $t \in (\sigma, t_{k+1}]$ as

$$\dot{\kappa}(\sigma + \tau) = \underbrace{\dot{\kappa}(\sigma)}_{=0} + \int_{\sigma}^{\sigma + \tau} \ddot{\kappa}(t) dt$$

$$\stackrel{\text{(A4)}}{\geq} \int_{\sigma}^{\sigma + \tau} (-\mu - M_2^+ + M_3^-(t - \sigma) + M_2^-) dt$$

$$= (-\mu - M_2^+ + M_2^-)\tau + \frac{1}{2}M_3^-\tau^2 \tag{A5}$$

and lower bound $\kappa(t)$ for $t \in (\sigma, t_{k+1}]$ as

$$\kappa(\sigma + \tau) = \kappa(\sigma) + \int_{\sigma}^{\sigma + \tau} \dot{\kappa}(t) dt$$

$$\stackrel{\text{(A5)}}{\geq} h(\sigma) + \int_{\sigma}^{\sigma + \tau} \left((-\mu - M_2^+ + M_2^-)(t - \sigma) + \frac{1}{2} M_3^- (t - \sigma)^2 \right) dt$$

$$= \kappa(\sigma) + \frac{1}{2} (-\mu - M_2^+ + M_2^-) \tau^2 + \frac{1}{6} M_3^- \tau^3$$
(A6)

Similarly, it follows from Eq. (23d) that

$$\ddot{\kappa}(\sigma - \tau) \ge -\mu + M_2^- - M_3^+ \tau - M_2^+ \tag{A7}$$

Thus, we can upper bound $\dot{\kappa}(t)$ for $t \in [t_k, \sigma)$ as

$$\dot{\kappa}(\sigma - \tau) = \underbrace{\dot{\kappa}(\sigma)}_{=0} - \int_{\sigma - \tau}^{\sigma} \dot{\kappa}(t) dt$$

$$\stackrel{\text{(A7)}}{\leq} - \int_{\sigma - \tau}^{\sigma} [-\mu - M_2^+ - M_3^+(\sigma - t) + M_2^-] dt$$

$$= (\mu + M_2^+ - M_2^-)\tau + \frac{1}{2}M_3^+\tau^2 \tag{A8}$$

^{††}https://youtu.be/geB-F5J4ZFI.

and lower bound $\kappa(t)$ for $t \in [t_k, \sigma)$ as

$$\kappa(\sigma - \tau) = \kappa(\sigma) - \int_{\sigma - \tau}^{\sigma} \dot{\kappa}(t) dt$$

$$\stackrel{\text{(A8)}}{\geq} \kappa(\sigma) - \int_{\sigma - \tau}^{\sigma} \left(-(-\mu - M_2^+ + M_2^-)(\sigma - t) + \frac{1}{2} M_3^+ (\sigma - t)^2 \right) dt$$

$$= \kappa(\sigma) + \frac{1}{2} (-\mu - M_2^+ + M_2^-) \tau^2 - \frac{1}{6} M_3^+ \tau^3$$
(A9)

We can then rearrange Eqs. (A6) and (A9) to

$$\kappa(\sigma) \le \kappa(\sigma + \tau) - \frac{1}{2}(-\mu - M_2^+ + M_2^-)\tau^2 - \frac{1}{6}M_3^-\tau^3$$
(A10)

$$\kappa(\sigma) \leq \kappa(\sigma - \tau) - \frac{1}{2} (-\mu - M_2^+ + M_2^-) \tau^2 + \frac{1}{6} M_3^+ \tau^3 \qquad (A11)$$

Let $\tau = t_{k+1} - \sigma$ in Eq. (A10) and $\tau = \sigma - t_k$ in Eq. (A11). Note that the bounds in Eqs. (A10) and (A11) must both apply simultaneously, or equivalently, whichever bound is tighter must apply. Thus, we obtain

$$\begin{split} &\kappa(\sigma) \overset{\text{(A10),(A11)}}{\leq} \\ &\min \left\{ -\delta_1 + \frac{1}{2} (\mu + M_2^+ - M_2^-) (t_{k+1} - \sigma)^2 - \frac{1}{6} M_3^- (t_{k+1} - \sigma)^3, \right. \\ &\left. -\delta_1 + \frac{1}{2} (\mu + M_2^+ - M_2^-) (\sigma - t_k)^2 + \frac{1}{6} M_3^+ (\sigma - t_k)^3 \right\} \overset{(24)}{\leq} 0 \end{split} \tag{A12}$$

Thus, because of the choice of δ_1 in Eq. (24), it is guaranteed that $\kappa(\sigma) \leq 0$ in Eq. (A12). It follows that $h(t) \leq h(\sigma) = \kappa(\sigma) \leq 0$ for all $t \in [t_k, t_{k+1}]$, or equivalently $x(t) \in \mathcal{H}(t)$ for all $t \in [t_k, t_{k+1}]$.

Proof of Theorem 2: The proof follows almost identical logic to that of Theorem 1, but instead of having $\kappa(t_k) \leq -\delta_1$ and $\kappa(t_{k+1}) \leq -\delta_1$, we end up with $\kappa(t_k) \leq -\Delta_2$ and $\kappa(t_{k+1}) \leq -\delta_2$. Thus, in place of Eq. (A12), we have

$$\kappa(\sigma) \le \min \left\{ -\delta_2 + \frac{1}{2} (\mu + M_2^+ - M_2^-) (t_{k+1} - \sigma)^2 - \frac{1}{6} M_3^- (t_{k+1} - \sigma)^3, -\Delta_2 + \frac{1}{2} (\mu + M_2^+ - M_2^-) (\sigma - t_k)^2 + \frac{1}{6} M_3^+ (\sigma - t_k)^3 \right\} \le 0$$
(A13)

Similar to in Theorem 1, the condition on Δ_2 and δ_2 in Eq. (25) ensures that $\kappa(\sigma) \leq 0$ regardless of the actual maximizer location $\sigma \in (t_k, t_{k+1})$. By the same logic as in Theorem 1, it follows that $\mathbf{x}(t) \in \mathcal{H}(t)$ for all $t \in [t_k, t_{k+1}]$.

Proof of Lemma 4: By assumption, $x(t_k) \in \mathcal{Q}(t_k)$ and $x(t_{k+1}) \in \mathcal{Q}(t_{k+1})$, so the trajectory can only leave \mathcal{Q} if there exists a local maximizer $t_s \in (t_k, t_{k+1})$ of κ such that $\kappa(t_s) > 0$. Thus, the rest of this proof proceeds by analyzing whether such a maximizer t_s can exist.

Note that, on the open interval (t_k, t_{k+1}) , the functions $\kappa, \dot{\kappa}$, and $\ddot{\kappa}$ are continuous in time, and therefore \dot{h} in Eq. (A1) is continuous as well. By assumption, σ is a maximizer of \dot{h} , so it follows that $\dot{h}(\sigma)=0$. Because of the form of \dot{h} in Eq. (A1), if $\dot{h}(\sigma)=0$ and $\dot{\kappa}(\sigma)\neq 0$, it must be that $\ddot{\kappa}(\sigma)=-\mu {\rm sign}(\dot{\kappa}(\sigma))$. That is, for a critical point of \dot{h} to occur at σ when $\dot{\kappa}(\sigma)\neq 0$, the second derivative of κ (e.g., angular acceleration) at σ must pass through one of two critical values, $\pm \mu$, depending on the sign of $\dot{\kappa}(\sigma)$. This yields the two cases below.

First, suppose that $\dot{\kappa}(\sigma) < 0$, which implies that $\ddot{\kappa}(\sigma) = \mu$. Thus, we can derive an expression for $\ddot{\kappa}(t)$ for t in a neighborhood of σ . Let $\tau \ge 0$ and it follows from Eq. (23a) that

$$\ddot{\kappa}(\sigma + \tau) \ge \mu + M_2^- + M_3^- \tau - M_2^+$$
 (A14)

Because of the assumed lower bound on μ , Eq. (A14) implies that $\ddot{\kappa}(\sigma + \tau) > 0$ for any $\tau \in (0, T)$. Similarly, it follows from Eq. (23d) that

$$\ddot{\kappa}(\sigma - \tau) \ge \mu + M_2^- - M_3^+ \tau - M_2^+$$
 (A15)

which implies that $\ddot{\kappa}(\sigma - \tau) > 0$ for any $\tau \in (0, T)$. Thus, by Eqs (A14) and (A15), $\ddot{\kappa}(t) > 0$ for all $t \in (t_k, t_{k+1})$ and therefore there can be no local maximizers of κ on (t_k, t_{k+1}) . Moreover, if there exists a time $t_s \in (t_k, t_{k+1})$ at which $\dot{\kappa}(t_s) = 0$, then t_s is unique and is a local minimizer of κ since $\ddot{\kappa}$ is strictly positive.

Second, suppose that $\dot{\kappa}(\sigma) > 0$, which implies that $\ddot{\kappa}(\sigma) = -\mu$. It follows from Eq. (23c) that

$$\ddot{\kappa}(\sigma - \tau) \le -\mu + M_2^+ - M_3^- \tau - M_2^- \tag{A16}$$

which implies that $\ddot{\kappa}(\sigma - \tau) < 0$ for all $\tau \in (0,T)$. Since $\dot{\kappa}(\sigma) > 0$ and $\ddot{\kappa}(\sigma - \tau) < 0$, it follows that $\dot{\kappa}(t) > 0$ for all $t \in [t_k,\sigma]$ and therefore there can be no local maximizers of κ on $[t_k,\sigma]$. Next, it follows from Eq. (23b) that

$$\ddot{\kappa}(\sigma + \tau) \le -\mu + M_2^+ + M_3^+ \tau - M_2^- \tag{A17}$$

which again implies that $\ddot{\kappa}(\sigma + \tau) < 0$ for all $\tau \in (0, T)$, and thus by Eqs. (A16) and (A17), $\ddot{\kappa}(t) < 0$ for all $t \in (t_k, t_{k+1})$. Thus, in this case, there may exist a local maximizer t_s of κ but only for $t_s \in (\sigma, t_{k+1}]$, such as shown by the green "x" in Fig. 4. If such a t_s exists, then $\dot{\kappa}(t_s) = 0$, and t_s is the unique maximizer of κ on $[t_k, t_{k+1}]$ since $\ddot{\kappa}$ is strictly negative. Going forward, we assume that such a t_s exists and now seek to ascertain its value.

From here, there are several possible ways to ensure that $\kappa(t) \le 0$ for all $t \in [t_k, t_{k+1}]$, and we only present one method. In our approach, we now shift our focus from the values of κ to the values of h. We will show that, for the choice of Δ_3 in Eq. (A34), it holds that $h(t) \le 0$ for all $t \in [t_k, t_{k+1}]$ and conclude that $x(t) \in \mathcal{Q}(t)$ for all $t \in [t_k, t_{k+1}]$ by applying Lemma 2.

Since $\dot{h}(\sigma) = 0$, we are interested in how positive $\dot{h}(t)$ can be for $t \in [t_k, \sigma]$ and how negative $\dot{h}(t)$ can be for $t \in [\sigma, t_{k+1}]$, from which we can derive a margin that ensures that $h(\sigma)$ does not exceed zero. To this end, it follows from Eq. (23d) that

$$\ddot{\kappa}(\sigma - \tau) \ge -\mu + M_2^- - M_3^+ \tau - M_2^+ \tag{A18}$$

Let $\dot{\kappa}(\sigma) = \gamma$ for $\gamma \in \mathbb{R}_{>0}$ at the maximizer σ of h, where the existence of $t_s \in (\sigma, t_{k+1})$ implies that γ is close to zero. First, for $t \in [t_k, \sigma]$, $\dot{\kappa}(t)$ is upper bounded as

$$\dot{\kappa}(\sigma - \tau) = \dot{\kappa}(\sigma) - \int_{\sigma - \tau}^{\sigma} \ddot{\kappa}(t) dt
\leq \gamma - \int_{\sigma - \tau}^{\sigma} -\mu + M_{2}^{-} - M_{2}^{+} - M_{3}^{+}(\sigma - t) dt
= \gamma + (\mu - M_{2}^{-} + M_{2}^{+})\tau + \frac{1}{2}M_{3}^{+}\tau^{2}$$
(A19)

Since we have $\dot{\kappa}(t) > 0$ for all $t \in [t_k, \sigma]$, it follows that $\dot{h}(t)$ is upper bounded by

$$\dot{h}(\sigma - \tau) \stackrel{\text{(A19)}}{=} \dot{\kappa}(\sigma - \tau) \left(1 + \frac{\ddot{\kappa}(\sigma - \tau)}{\mu} \right) \\
\stackrel{\text{(A19)}}{\leq} \left(\gamma + (\mu - M_2^- + M_2^+) \tau \right. \\
+ \frac{1}{2} M_3^+ \tau^2 \left(\frac{M_2^+ - M_3^- \tau - M_2^-}{\mu} \right) \tag{A20}$$

Next, similar to Eq. (A18), for $t \in [\sigma, t_{k+1}], \dot{\kappa}(t)$ is upper bounded by

$$\begin{split} \dot{\kappa}(\sigma + \tau) &= \dot{\kappa}(\sigma) + \int_{\sigma}^{\sigma + \tau} \ddot{\kappa}(t) \, \mathrm{d}t \\ &\stackrel{\text{(A17)}}{\leq} \gamma + \int_{\sigma}^{\sigma + \tau} -\mu + M_2^+ - M_2^- + M_3^+(t - \sigma) \, \mathrm{d}t \\ &= \gamma - (\mu + M_2^- - M_2^+)\tau + \frac{1}{2}M_3^+\tau^2 \end{split} \tag{A21}$$

We now divide the interval $[\sigma, t_{k+1}]$ into two intervals $[\sigma, t_s)$ and $(t_s, t_{k+1}]$ because, unlike the upper bound in Eq. (A20), our lower bounds for \dot{h} in Eq. (A1) will be different before and after $\dot{\kappa}$ changes from positive to negative at t_s . For the interval $t \in [\sigma, t_s)$ where $\dot{\kappa}(t) > 0$, $\dot{h}(t)$ is minimized by minimizing $\ddot{\kappa}(t)$, so we note that Eq. (23a) lower bounds $\ddot{\kappa}(t)$ as

$$\ddot{\kappa}(\sigma + \tau) \ge -\mu + M_2^- + M_3^- \tau - M_2^+$$
 (A22)

Thus, during the interval $t \in [\sigma, t_s)$ where $\dot{\kappa}(t) > 0$, it follows that $\dot{h}(t)$ is lower bounded by

$$\dot{h}(\sigma + \tau) \stackrel{\text{(A21)}, \text{(A22)}}{=} \dot{\kappa}(\sigma + \tau) \left(1 + \frac{\ddot{\kappa}(\sigma - \tau)}{\mu} \right) \\
\stackrel{\text{(A21)}, \text{(A22)}}{\geq} \left(\gamma - (\mu + M_2^- - M_2^+)\tau + \frac{1}{2}M_3^+\tau^2 \right) \left(\frac{M_2^- + M_3^-\tau - M_2^+}{\mu} \right) \\
(A23)$$

To take into account the interval $t \in (t_s, t_{k+1}]$ where $\dot{\kappa}(t) < 0$, instead of the upper bound Eq. (A17), we will utilize the following lower bound for $\dot{\kappa}$:

$$\dot{\kappa}(\sigma + \tau) = \dot{\kappa}(\sigma) + \int_{\sigma}^{\sigma + \tau} \ddot{\kappa}(t) dt$$

$$\stackrel{\text{(A22)}}{\geq} \gamma + \int_{\sigma}^{\sigma + \tau} -\mu + M_{2}^{-} - M_{2}^{+} + M_{3}^{-}(t - \sigma) dt$$

$$= \gamma - (\mu - M_{2}^{-} + M_{2}^{+})\tau + \frac{1}{2}M_{3}^{-}\tau^{2} \tag{A24}$$

Finally, during the interval $t \in (t_s, t_{k+1}]$ where $\dot{\kappa}(t) < 0$, it follows that $\dot{h}(t)$ is lower bounded as

$$\begin{split} \dot{h}(\sigma+\tau) &\stackrel{\text{(A24)}}{=} \dot{\kappa}(\sigma+\tau) \left(1 - \frac{\ddot{\kappa}(\sigma-\tau)}{\mu}\right) \\ &\stackrel{\text{(A24)},\text{(A22)}}{\geq} \left(\gamma - (\mu - M_2^- + M_2^+)\tau + \frac{1}{2}M_3^-\tau^2\right) \left(2 - \frac{M_2^- + M_3^-\tau - M_2^+}{\mu}\right) \end{split} \tag{A25}$$

Next, given the bounds for $\dot{h}(t)$ in Eqs. (A20), (A23), and (A25), we seek to upper bound $h(\sigma) - h(t_k)$ and $h(\sigma) - h(t_{k+1})$. Starting with the latter, we have that

$$h(\sigma) - h(t_{k+1}) = -\int_{\sigma}^{t_s} \dot{h}(t) dt - \int_{t_s}^{t_{k+1}} \dot{h}(t) dt$$

$$\leq -\int_{\sigma}^{t_s} [\dot{h}(t) \operatorname{as in} (A23)] dt$$

$$-\int_{t_s}^{t_{k+1}} [\dot{h}(t) \operatorname{as in} (A25)] dt \qquad (A26)$$

where $t_s \in (\sigma, t_{k+1}]$ is an unknown parameter. Because of the disturbance, we cannot develop an exact expression for t_s as a function of γ [this is why τ_1, τ_2 will be free optimization parameters in Eq. (A34)], but we can develop lower and upper bounds on t_s for the computation of Eq. (A26). Possible trajectories of $\dot{\kappa}(\sigma + \tau)$ are visualized in Fig. A1. At t_s , $\dot{\kappa}(t_s) = 0$, where $\dot{\kappa}$ is bounded by Eqs. (A21) and (A24), so all candidate values of t_s must lie between the roots of the bounding functions (A21) and (A24). Since we assumed that $M_3^- < 0$, the red line (A24) is a concave downward quadratic polynomial. Since $\dot{\kappa}(t) > 0$ for $t \in [\sigma, t_s)$, it follows that t_s must lie to the right of the second root of Eq. (A24) (dashed red vertical line in Fig. A1), denoted $t_s : \mathbb{R}_{>0} \to \mathbb{R}$:

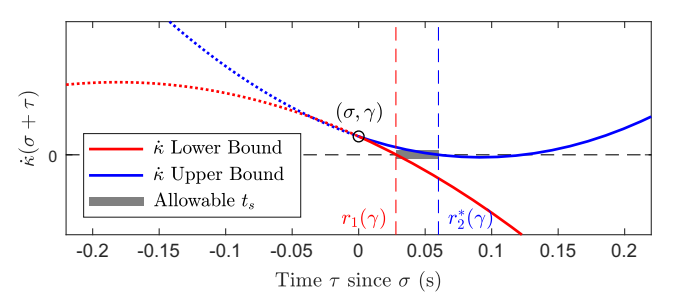


Fig. A1 Visualization of the lower and upper bounds on $\dot{\kappa}(\sigma+\tau)$ imposed by Eq. (A24) (red solid line) and Eq. (A21) (blue solid line), respectively, and how this results in a finite interval of possible roots of $\dot{\kappa}$

$$t_{s} - \sigma \stackrel{\text{(A24)}}{\geq} r_{1}(\gamma) \triangleq \frac{1}{M_{3}^{-}} \left[(\mu + M_{2}^{-} - M_{2}^{+}) - \sqrt{(\mu + M_{2}^{-} - M_{2}^{+})^{2} - 2M_{3}^{-} \gamma} \right]$$
(A27)

Similarly, since we assumed that $M_3^+ > 0$, the blue line (A21) is a concave upward quadratic polynomial, and since $\dot{\kappa}(t) < 0$ for $t \in (t_s, t_{k+1})$, it follows that t_s must lie to the left of the first root of Eq. (A21) (dashed blue vertical line in Fig. A1), denoted $r_2^* : \mathbb{R}_{\geq 0} \to \mathbb{R}$:

$$r_2^*(\gamma) \triangleq \frac{1}{M_3^+} \left[(\mu - M_2^- + M_2^+) - \sqrt{(\mu - M_2^- + M_2^+)^2 - 2M_3^+ \gamma} \right]$$
(A28)

The time t_s must also occur inside the present time step, so we define the bound $r_2: \mathbb{R}_{\geq 0} \times \mathbb{R}_{\geq 0} \to \mathbb{R}$ as follows, and conclude that

$$\begin{split} t_s &- \sigma \overset{\text{(A21)}}{\leq} r_2(\gamma, \sigma - t_k) \\ &\triangleq \begin{cases} \min\{r_2^*(\gamma), T - (\sigma - t_k)\} & \text{if } \gamma \leq (\mu - M_2^- + M_2^+)^2/(2M_3^+) \\ T - (\sigma - t_k) & \text{else} \end{cases} \end{split}$$

The second case of Eq. (A29) occurs when γ is such that Eq. (A28) is nonreal, in which case t_s is instead upper bounded by the length of the time step. Note that the bounds (A27) and (A29) greatly simplify the complete relationship between t_s and γ , but accounting for all possible curves of κ in a neighborhood of t_s would require more assumptions about the disturbance and would make this proof far more complex. Instead, we choose to treat t_s and γ as free parameters with minimal coupling to each other except that in Eq. (A27) and (A29), so that Eq. (A26) is computable. We then simplify the right hand side of Eq. (A26) and assign the result to the function $d_{\text{right}}: \mathbb{R}_{\geq 0} \times \mathbb{R}_{\geq 0} \times \mathbb{R}_{\geq 0} \to \mathbb{R}$ defined as

$$\begin{split} d_{\text{right}}(\gamma,\tau_{1},\tau_{2}) &\triangleq \frac{(M_{3}^{-})^{2}}{8\mu} \left(\tau_{1}^{4} - \tau_{2}^{4}\right) - \frac{M_{3}^{-}M_{3}^{+}}{8\mu} \tau_{2}^{4} \\ &+ \left[\frac{M_{3}^{-}(M_{2}^{-} - M_{2}^{+})}{2\mu} - \frac{2M_{3}^{-}}{3}\right] \left(\tau_{1}^{3} - \tau_{2}^{3}\right) \\ &+ \frac{1}{6\mu} \left[2M_{3}^{-}(M_{2}^{-} - M_{2}^{+} + \mu) - M_{3}^{+}(M_{2}^{-} - M_{2}^{+})\right] \tau_{2}^{3} \\ &+ \frac{1}{2\mu} \left[(M_{2}^{+} - M_{2}^{-} + 2\mu)(M_{2}^{+} - M_{2}^{-} + \mu) + M_{3}^{-}\gamma\right] \left(\tau_{1}^{2} - \tau_{2}^{2}\right) \\ &+ \frac{1}{2\mu} \left[(M_{2}^{-} - M_{2}^{+})(M_{2}^{-} - M_{2}^{+} + \mu) - M_{3}^{-}\gamma\right] \tau_{2}^{2} \\ &+ \frac{\gamma}{\mu} (M_{2}^{-} - M_{2}^{+} - 2\mu)(\tau_{1} - \tau_{2}) - \frac{1}{\mu} \left(\gamma(M_{2}^{-} - M_{2}^{+})\right) \tau_{2} \end{split} \tag{A30}$$

so that Eq. (A26) simplifies to

$$h(\sigma) - h(t_{k+1}) \le d_{\text{right}}(\gamma, t_{k+1} - \sigma, t_s - \sigma) \tag{A31}$$

where the third argument $t_s - \sigma$ is bounded by Eqs. (A27) and (A29). Similar to Eq. (A26), we can bound $h(\sigma) - h(t_k)$ as

$$h(\sigma) - h(t_k) = \int_{t_k}^{\sigma} \dot{h}(t) \le \int_{t_k}^{\sigma} [\dot{h}(t) \operatorname{as in} (A20)] dt = d_{\operatorname{left}}(\gamma, \sigma - t_k)$$
(A32)

where we do not need to break the integral into two parts here because $\dot{\kappa}(t)$ does not change signs on $[t_k, \sigma]$. We then define the function $d_{\text{left}}: \mathbb{R}_{\geq 0} \times \mathbb{R}_{\geq 0} \to \mathbb{R}$ as the simplification of the integral in Eq. (A32) as follows:

$$\begin{split} d_{\mathrm{left}}(\gamma,\tau) &\triangleq -\frac{\tau^4}{8\mu}(M_3^- M_3^+) - \frac{\tau^3}{6\mu}(2M_3^- (M_2^+ - M_2^- + \mu) \\ &+ M_3^+ (M_2^- - M_2^+)) - \frac{\tau^2}{2\mu}((M_2^- - M_2^+)(M_2^+ - M_2^- + \mu) \\ &+ M_3^- \gamma) - \frac{\gamma\tau}{\mu}(M_2^- - M_2^+) \end{split} \tag{A33}$$

Both Eqs. (A31) and (A32) must apply simultaneously, so we define Δ_3 below as a maximization of the lesser of d_{left} and d_{right} , subject to the constraints on $t_s - \sigma$ in Eqs. (A26) and (A29). Furthermore, the maximizer σ of h must occur in the present time step, so $\sigma - t_k \in [0, T]$, and γ must be positive. Let $\tau_1 = \sigma - t_k$ and $\tau_2 = t_s - \sigma$, and finally define

$$\Delta_{3} \triangleq \max_{\substack{\gamma \in [0,\infty) \\ \tau_{\gamma} \in [0,T]}} \left(\min\{d_{\text{left}}(\gamma, \tau_{1}), d_{\text{right}}(\gamma, T - \tau_{1}, \tau_{2})\} \right)$$
(A34)

Note that although γ is not upper bounded in Eq. (A34), in practice there is a maximum value of γ for which the interval $[r_1(\gamma), r_2(\gamma, \sigma - t_k)]$ is nonempty. Finally, using both bounds (A31) and (A32), the maximum value of h is bounded by

$$\begin{split} h(\sigma) &\overset{\text{(A31),(A32)}}{\leq} \min\{h(t_k) + d_{\text{left}}(\gamma, \sigma - t_k), \\ & h(t_{k+1}) + d_{\text{right}}(\gamma, t_{k+1} - \sigma, t_s - \sigma)\} \\ &\leq -\Delta_3 + \min\{d_{\text{left}}(\gamma, \sigma - t_k), d_{\text{right}}(\gamma, t_{k+1} - \sigma, t_s - \sigma)\} \overset{\text{(A34)}}{\leq} 0 \end{split} \tag{A35}$$

so $x(t) \in \mathcal{H}(t)$ for all $t \in [t_k, t_{k+1}]$. By Lemma 2, $x(t) \in \mathcal{Q}(t)$ for all $t \in [t_k, t_{k+1}]$ too. In summary, we have shown that 1) when $\dot{\kappa}(\sigma) < 0$, no maximizer t_s of κ can occur, and 2) when $\dot{\kappa}(\sigma) > 0$, only one maximizer t_s of κ can occur and by Eq. (A35) and Lemma 2, $\kappa(t_s) < 0$, so $x(t) \in \mathcal{Q}(t)$ for all $t \in [t_k, t_{k+1}]$ in all cases where $\dot{\kappa}(\sigma) \neq 0$.

Proof of Theorem 3: By assumption, $\kappa(t_k) \leq 0$, $h(t_k) \leq -\Delta_2 \leq 0$, $\kappa(t_{k+1}) \leq -\delta_2 \leq 0$, and $h(t_{k+1}) \leq -\Delta_2 \leq 0$. Thus, $\kappa(t)$ can only exit \mathcal{Q} if there is a local maximizer t_s of κ for $t_s \in (t_k, t_{k+1})$. As a result of Lemma 2, it is only possible for $\kappa(t_s) > 0$ to occur if there also exists a local maximizer σ of h for $\sigma \in (t_k, t_{k+1})$ such that $h(\sigma) > 0$, where it is possible that $\sigma = t_s$. Suppose the existence of both t_s and σ , where neither is necessarily unique. If there exists a maximizer σ of h such that $\kappa(\sigma) \neq 0$, then Lemma 4 implies that t_s is unique and that $\kappa(t_s) \leq 0$.

Next, if every maximizer σ of h satisfies $\dot{\kappa}(\sigma) = 0$, then Theorem 2 implies that $\kappa(t_s) \leq 0$ for every t_s , where $t_s = \sigma$. Finally, if there is one or more maximizers σ_1 of h such that $\dot{\kappa}(\sigma_1) = 0$, and one maximizer σ_2 of h such that $\dot{\kappa}(\sigma_2) \neq 0$, then by the first paragraph, t_s is unique and $\kappa(t_s) \leq 0$, and it follows that σ_1 is unique and $\sigma_1 = t_s$. That is, the conditions presented so far do not preclude the possibility of the cases described in Lemma 3 and Lemma 4 both occurring in the

same time step, but in this case, safety is ensured by Lemma 4 alone. Since $\kappa(t_s) \leq 0$ for every maximizer t_s of κ , it follows that $\kappa(t) \leq 0$ for all $t \in [t_k, t_{k+1}]$, and thus $\kappa(t) \in \mathcal{Q}(t)$ for all $t \in [t_k, t_{k+1}]$.

Proof of Theorem 4: First, note that we can upper bound the evolution of $\dot{\kappa}$ and κ between time steps as follows:

$$\dot{\kappa}(t_k + \tau) = \dot{\kappa}(t_k) + \int_{t_k}^{t_k + \tau} \ddot{\kappa}(t) dt$$

$$\stackrel{(22a)}{\leq} \int_{t_k}^{t_k + \tau} \psi(t_k) + M_2^+ + M_3^+(t - t_k) dt$$

$$= \dot{\kappa}(t_k) + \psi(t_k)\tau + M_2^+\tau + \frac{1}{2}M_3^+\tau^2 \tag{A36}$$

$$\kappa(t_{k}+\tau) = \kappa(t_{k}) + \int_{t_{k}}^{t_{k}+\tau} \dot{\kappa}(t_{k}) + \int_{t_{k}}^{\tau_{1}} \ddot{\kappa}(t) dt d\tau_{1}$$

$$\stackrel{(22a)}{\leq} \kappa(t_{k}) + \int_{t_{k}}^{t_{k}+\tau} \dot{\kappa}(t_{k}) + \int_{t_{k}}^{\tau_{1}} \psi(t_{k}) + M_{2}^{+} + M_{3}^{+}(t-t_{k}) dt d\tau_{1}$$

$$= p_{\kappa}(t_{k},\tau) \tag{A37}$$

Thus, p_{κ} in Eq. (27) is an upper bound on $\kappa(t_k + \tau)$, and Eq. (A36) is an upper bound on $\dot{\kappa}(t_k + \tau)$. Since h in Eq. (13) is monotonically increasing in both κ and $\dot{\kappa}$, it follows that p_h in Eq. (28) is an upper bound on $h(t_k + \tau)$. Since $t_{k+1} = t_k + T$, it follows that Eq. (29a) implies $\mathbf{x}(t_{k+1}) \in \mathcal{Q}^{\delta_2}(t_{k+1})$ and Eq. (29b) implies $\mathbf{x}(t_{k+1}) \in \mathcal{H}^{\Delta_2}(t_{k+1})$, or equivalently $\mathbf{x}(t_{k+1}) \in \mathcal{Z}(t_{k+1})$. Since this holds for every $k \in \mathbb{N}$, Theorem 3 implies that $\mathbf{x}(t) \in \mathcal{Q}(t)$ for all $t \in \mathbb{T}$.

Proof of Theorem 5: First, note that we can upper bound the evolution of η between time steps as follows:

$$\eta(t_{k} + \tau) = \eta(t_{k}) + \int_{t_{k}}^{t_{k} + \tau} \dot{\eta}(t_{k}) + \int_{t_{k}}^{\tau_{1}} \ddot{\eta}(t_{k} + \tau_{2}) d\tau_{2} d\tau_{1}
\stackrel{(36)}{\leq} \eta(t_{k}) + \int_{t_{k}}^{t_{k} + \tau} \dot{\eta}(t_{k}) + \int_{t_{k}}^{\tau_{1}} M_{2} d\tau_{2} d\tau_{1}
\stackrel{(34)}{\leq} \eta(t_{k}) + \int_{t_{k}}^{t_{k} + \tau} \phi(t_{k}) + M_{1} + M_{2}\tau_{1} d\tau_{1} \stackrel{(38)}{\leq} p_{\eta}(t_{k}, \tau)$$
(A38)

It follows that if $p_{\eta}(t_k, \tau) \leq 0$, then $\eta(t_k + \tau) \leq 0$ and thus $\boldsymbol{x}(t_k + \tau) \in \mathcal{V}(t_k + \tau)$. Note that p_{η} in Eq. (38) is a concave upward quadratic in τ (since M_2 is assumed to be nonnegative), so if $p_{\eta}(t_k, 0) = \eta(t_k) \leq 0$ and $p_{\eta}(t_k, T) \leq 0$, then $\eta(t_k + \tau) \leq p_{\eta}(t_k, \tau) \leq p_{\eta}(t_k, T) \leq 0$ for all $\tau \in [0, T]$. Since we assumed $\boldsymbol{x}(t_0) \in \mathcal{V}(t_0)$, or equivalently $p_{\eta}(t_0, 0) = \eta(t_0) \leq 0$, and since Eq. (A38) implies $p_{\eta}(t_k, T) \leq 0$ for all $k \in \mathbb{N}$, it follows that $\eta(t) \leq 0$ for all $t \in \mathbb{T}$, or equivalently, $\boldsymbol{x}(t) \in \mathcal{V}(t)$ for all $t \in \mathbb{T}$.

Proof of Corollary 1: Similar to Eq. (A38), $p_{\eta}^{\text{alt}}(t_k, \tau)$ in Eq. (43) is an upper bound on $\eta(t_k + \tau)$. By Eq. (14), \boldsymbol{u} is constant between time steps and therefore the quadratic coefficient of p_{η}^{alt} given by $\phi_1(\boldsymbol{u}(t_k)) + M_2^{\text{alt}}$ is constant. Because ϕ_1 maps to $\mathbb{R}_{\geq 0}$ and $M_2^{\text{alt}} \geq 0$, the coefficient $\phi_1(\boldsymbol{u}(t_k)) + M_2^{\text{alt}}$ is also nonnegative. Thus, $p_{\eta}^{\text{alt}}(t_k, \tau)$ is a concave upward quadratic polynomial in τ , so if $\eta(t_k) \leq 0$ and $p_{\eta}^{\text{alt}}(t_k, T) \leq 0$, then it follows by the same logic as Theorem 5 that $\boldsymbol{x}(t) \in \mathcal{V}(t)$ for all $t \in \mathbb{T}$.

Acknowledgments

This research was supported by the United States National Science Foundation under grant no. 1942907 and under the Graduate Research Fellowship Program, and by the University of Michigan François Xavier Bagnoud Fellowship. The authors wish to thank Rohit Gupta of the Indian Institute of Technology Bombay for providing the optimization code used to simulate the controller in [12], and Eric Stoneking of the NASA Goddard Space Flight

Center for developing and distributing the "42" Spacecraft Simulation platform [44].

References

- [1] Kim, Y., and Mesbahi, M., "Quadratically Constrained Attitude Control via Semidefinite Programming," *IEEE Transactions on Automatic Control*, Vol. 49, No. 5, 2004, pp. 731–735. https://doi.org/10.1109/TAC.2004.825959
- [2] Kim, Y., Mesbahi, M., Singh, G., and Hadaegh, F. Y., "On the Convex Parameterization of Constrained Spacecraft Reorientation," *IEEE Transactions on Aerospace and Electronic Systems*, Vol. 46, No. 3, 2010, pp. 1097–1109. https://doi.org/10.1109/TAES.2010.5545176
- [3] Weiss, A., Leve, F., Baldwin, M., Forbes, J. R., and Kolmanovsky, I., "Spacecraft Constrained Attitude Control Using Positively Invariant Constraint Admissible Sets on SO(3) x R3," 2014 American Control Conference, IEEE, New York, 2014, pp. 4955–4960. https://doi.org/10.1109/ACC.2014.6858878
- [4] Tan, X., Berkane, S., and Dimarogonas, D. V., "Constrained Attitude Maneuvers on SO(3): Rotation Space Sampling, Planning and Low-Level Control," *Automatica*, Vol. 112, Feb. 2020, Paper 108659. https://doi.org/10.1016/j.automatica.2019.108659
- [5] Reynolds, T. P., Szmuk, M., Malyuta, D., Mesbahi, M., Açıkmeşe, B., and Carson, J. M., "Dual Quaternion-Based Powered Descent Guidance with State-Triggered Constraints," *Journal of Guidance, Control, and Dynamics*, Vol. 43, No. 9, 2020, pp. 1584–1599. https://doi.org/10.2514/1.G004536
- [6] Sun, C., and Dai, R., "Spacecraft Attitude Control under Constrained Zones via Quadratically Constrained Quadratic Programming," AIAA Guidance, Navigation, and Control Conference, AIAA Paper 2015-2010, 2015. https://doi.org/10.2514/6.2015-2010
- [7] Calaon, R., and Schaub, H., "Constrained Attitude Maneuvering via Modified-Rodrigues-Parameter-Based Motion Planning Algorithms," *Journal of Spacecraft and Rockets*, Vol. 59, No. 4, 2022, pp. 1342–1356. https://doi.org/10.2514/1.A35294
- [8] Kjellberg, H. C., and Lightsey, E. G., "Discretized Constrained Attitude Pathfinding and Control for Satellites," *Journal of Guidance, Control, and Dynamics*, Vol. 36, No. 5, 2013, pp. 1301–1309. https://doi.org/10.2514/1.60189
- [9] Tanygin, S., "Fast Autonomous Three-Axis Constrained Attitude Pathfinding and Visualization for Boresight Alignment," *Journal of Guidance, Control, and Dynamics*, Vol. 40, No. 2, 2017, pp. 358–370. https://doi.org/10.2514/1.G001801
- [10] Feron, E., Dahleh, M., Frazzoli, E., and Kornfeld, R., "A Randomized Attitude Slew Planning Algorithm for Autonomous Spacecraft," AIAA Guidance, Navigation, and Control Conference and Exhibit, AIAA Paper 2001-4155, 2001. https://doi.org/10.2514/6.2001-4155
- [11] Kalabić, U., Gupta, R., Di Cairano, S., Bloch, A., and Kolmanovsky, I., "Constrained Spacecraft Attitude Control on SO(3) Using Reference Governors and Nonlinear Model Predictive Control," 2014 American Control Conference, IEEE, New York, 2014, pp. 5586–5593. https://doi.org/10.1109/ACC.2014.6858865
- [12] Gupta, R., Kalabić, U. V., Di Cairano, S., Bloch, A. M., and Kolmanovsky, I. V., "Constrained Spacecraft Attitude Control on SO(3) Using Fast Nonlinear Model Predictive Control," 2015 American Control Conference, IEEE, New York, 2015, pp. 2980–2986. https://doi.org/10.1109/ACC.2015.7171188
- [13] Lee, D. Y., Gupta, R., Kalabić, U. V., Di Cairano, S., Bloch, A. M., Cutler, J. W., and Kolmanovsky, I. V., "Constrained Attitude Maneuvering of a Spacecraft with Reaction Wheel Assembly by Nonlinear Model Predictive Control," 2016 American Control Conference, IEEE, New York, 2016, pp. 4960–4965. https://doi.org/10.1109/ACC.2016.7526139
- [14] Lee, D. Y., Gupta, R., Kalabić, U. V., Di Cairano, S., Bloch, A. M., Cutler, J. W., and Kolmanovsky, I. V., "Geometric Mechanics Based Nonlinear Model Predictive Spacecraft Attitude Control with Reaction Wheels," *Journal of Guidance, Control, and Dynamics*, Vol. 40, No. 2, 2017, pp. 309–319. https://doi.org/10.2514/1.G001923
- [15] Lourenço, P., Franco, J., Milhano, T., and Branco, J., "Model Predictive Control for On-Board-Optimized Attitude Guidance for Cometary Fly-By-Problem Statement, Solutions and V&V Process," *Proceedings of* the 8th International Conference on Astrodynamics Tools and Techniques, European Space Agency, 2021. https://doi.org/10.5281/zenodo.6411680

- [16] Yang, J., Duan, Y., Ben-Larbi, M. K., and Stoll, E., "Potential Field-Based Sliding Surface Design and Its Application in Spacecraft Constrained Reorientation," *Journal of Guidance, Control, and Dynamics*, Vol. 44, No. 2, 2021, pp. 399–409. https://doi.org/10.2514/1.G005026
- [17] Shen, Q., Yue, C., Goh, C. H., Wu, B., and Wang, D., "Rigid-Body Attitude Stabilization with Attitude and Angular Rate Constraints," *Automatica*, Vol. 90, April 2018, pp. 157–163. https://doi.org/10.1016/j.automatica.2017.12.029
- [18] Kang, Z., Shen, Q., and Wu, S., "Constrained Attitude Control of Over-Actuated Spacecraft Subject to Instrument Pointing Direction Deviation," *IEEE Control Systems Letters*, Vol. 5, No. 6, 2021, pp. 1958–1963. https://doi.org/10.1109/LCSYS.2020.3044984
- [19] Nicotra, M. M., Liao-McPherson, D., Burlion, L., and Kolmanovsky, I. V., "Spacecraft Attitude Control with Nonconvex Constraints: An Explicit Reference Governor Approach," *IEEE Transactions on Automatic Control*, Vol. 65, No. 8, 2020, pp. 3677–3684. https://doi.org/10.1109/TAC.2019.2951303
- [20] McInnes, C. R., "Large Angle Slew Maneuvers with Autonomous Sun Vector Avoidance," *Journal of Guidance, Control, and Dynamics*, Vol. 17, No. 4, 1994, pp. 875–877. https://doi.org/10.2514/3.21283
- [21] Lee, U., and Mesbahi, M., "Spacecraft Reorientation in Presence of Attitude Constraints via Logarithmic Barrier Potentials," *Proceedings of the 2011 American Control Conference*, IEEE, New York, 2011, pp. 450–455. https://doi.org/10.1109/ACC.2011.5991284
- [22] Lee, U., and Mesbahi, M., "Feedback Control for Spacecraft Reorientation Under Attitude Constraints via Convex Potentials," *IEEE Transactions on Aerospace and Electronic Systems*, Vol. 50, No. 4, 2014, pp. 2578–2592. https://doi.org/10.1109/TAES.2014.120240
- [23] Dong, H., Zhao, X., and Yang, H., "Reinforcement Learning-Based Approximate Optimal Control for Attitude Reorientation Under State Constraints," *IEEE Transactions on Control Systems Technology*, Vol. 29, No. 4, 2021, pp. 1664–1673.
- https://doi.org/10.1109/TCST.2020.3007401
 [24] Diaz Ramos, M., and Schaub, H., "Kinematic Steering Law for Conically Constrained Torque-Limited Spacecraft Attitude Control," *Journal of Guidance, Control, and Dynamics*, Vol. 41, No. 9, 2018, pp. 1990–2001. https://doi.org/10.2514/1.G002873
- [25] Tan, X., and Dimarogonas, D. V., "Construction of Control Barrier Function and C² Reference Trajectory for Constrained Attitude Maneuvers," 2020 59th IEEE Conference on Decision and Control, IEEE, New York, 2020, pp. 3329–3334. https://doi.org/10.1109/CDC42340.2020.9304324
- [26] Breeden, J., and Panagou, D., "Quadratic Programs for High Relative Degree Spatial Constraints and Spatiotemporal Specifications with Spacecraft Applications," 2020 59th IEEE Conference on Decision and Control, IEEE, New York, 2020, pp. 1496–1502. https://doi.org/10.1109/CDC42340.2020.9304162
- [27] Wu, G., and Sreenath, K., "Safety-Critical and Constrained Geometric Control Synthesis Using Control Lyapunov and Control Barrier Functions for Systems Evolving on Manifolds," 2015 American Control Conference, IEEE, New York, 2015, pp. 2038–2044.
- [28] Ibuki, T., Wilson, S., Ames, A. D., and Egerstedt, M., "Distributed Collision-Free Motion Coordination on a Sphere: A Conic Control Barrier Function Approach," *IEEE Control Systems Letters*, Vol. 4, No. 4, 2020, pp. 976–981. https://doi.org/10.1109/LCSYS.2020.2997952
- [29] Breeden, J., Garg, K., and Panagou, D., "Control Barrier Functions in Sampled-Data Systems," *IEEE Control Systems Letters*, Vol. 6, April 2022, pp. 367–372. https://doi.org/10.1109/LCSYS.2021.3076127
- [30] Mitchell, I. M., Budzis, J., and Bolyachevets, A., "Invariant, Viability and Discriminating Kernel Under-Approximation via Zonotope Scaling," Proceedings of the 22nd ACM International Conference on Hybrid Systems: Computation and Control, Assoc. for Computing Machinery, New York, 2019, pp. 268–269. https://doi.org/10.1145/3302504.3313354
- [31] Garg, K., and Panagou, D., "Robust Control Barrier and Control Lyapunov Functions with Fixed-Time Convergence Guarantees," 2021 American Control Conference, IEEE, New York, 2021, pp. 2292–2297. https://doi.org/10.23919/ACC50511.2021.9482751
- [32] Jankovic, M., "Robust Control Barrier Functions for Constrained Stabilization of Nonlinear Systems," Automatica, Vol. 96, Oct. 2018,

- pp. 359-367.
- https://doi.org/10.1016/j.automatica.2018.07.004
- [33] Breeden, J., and Panagou, D., "Robust Control Barrier Functions Under High Relative Degree and Input Constraints for Satellite Trajectories," *Automatica*, Vol. 155, Sept. 2023, Paper 111109. https://doi.org/10.1016/j.automatica.2023.111109
- [34] Shaw Cortez, W., Oetomo, D., Manzie, C., and Choong, P., "Control Barrier Functions for Mechanical Systems: Theory and Application to Robotic Grasping," *IEEE Transactions on Control Systems Technology*, Vol. 29, No. 2, 2021, pp. 530–545. https://doi.org/10.1109/TCST.2019.2952317
- [35] Ames, A. D., Coogan, S., Egerstedt, M., Notomista, G., Sreenath, K., and Tabuada, P., "Control Barrier Functions: Theory and Applications," 2019 18th European Control Conference, IEEE, New York, 2019, pp. 3420–3431. https://doi.org/10.23919/ECC.2019.8796030
- [36] Tan, X., and Dimarogonas, D. V., "Compatibility Checking of Multiple Control Barrier Functions for Input Constrained Systems," 2022 IEEE 61st Conference on Decision and Control (CDC), IEEE, New York, 2022, pp. 939–944. https://doi.org/10.1109/CDC51059.2022.9993001
- [37] Breeden, J., and Panagou, D., "Compositions of Multiple Control Barrier Functions Under Input Constraints," 2023 American Control Conference, IEEE, New York, 2023, pp. 3688–3695.
- [38] Nguyen, Q., and Sreenath, K., "Exponential Control Barrier Functions for Enforcing High Relative-Degree Safety-Critical Constraints," 2016 American Control Conference, IEEE, New York, 2016, pp. 322– 328.
 - https://doi.org/10.1109/ACC.2016.7524935

- [39] Squires, E., Pierpaoli, P., and Egerstedt, M., "Constructive Barrier Certificates with Applications to Fixed-Wing Aircraft Collision Avoidance," 2018 IEEE Conference on Control Technology and Applications, IEEE, New York, 2018, pp. 1656–1661. https://doi.org/10.1109/CCTA.2018.8511342
- [40] Xiao, W., and Belta, C., "Control Barrier Functions for Systems with High Relative Degree," 2019 IEEE 58th Conference on Decision and Control, IEEE, New York, 2019, pp. 474–479. https://doi.org/10.1109/CDC40024.2019.9029455
- [41] Breeden, J., and Panagou, D., "High Relative Degree Control Barrier Functions Under Input Constraints," 2021 60th IEEE Conference on Decision and Control, IEEE, New York, 2021, pp. 6119–6124. https://doi.org/10.1109/CDC45484.2021.9683705
- [42] Markley, F. L., and Crassidis, J. L., Fundamentals of Spacecraft Attitude Determination and Control, Springer–Verlag, New York, 2014, Chap. 3. https://doi.org/10.1007/978-1-4939-0802-8
- [43] Karpenko, M., Bhatt, S., Bedrossian, N., and Ross, I. M., "Flight Implementation of Shortest-Time Maneuvers for Imaging Satellites," *Journal of Guidance, Control, and Dynamics*, Vol. 37, No. 4, 2014, pp. 1069–1079. https://doi.org/10.2514/1.62867
- [44] Stoneking, E., "42: An Open-Source Simulation Tool for Study and Design of Spacecraft Attitude Control Systems," NASA Goddard Space Flight Center GSFC-E-DAA-TN52069, 2018, https://ntrs.nasa.gov/ citations/20180000954.
- [45] Stellato, B., Banjac, G., Goulart, P., Bemporad, A., and Boyd, S., "OSQP: An Operator Splitting Solver for Quadratic Programs," *Mathematical Programming Computation*, Vol. 12, No. 4, 2020, pp. 637–672. https://doi.org/10.1007/s12532-020-00179-2